A review of processing strategies to generate melt-blown nano/microfiber mats for high-efficiency filtration applications

Kara Y., Molnár K.

Accepted for publication in Journal of Industrial Textiles
Published in 2021
DOI: https://doi.org/10.1177/15280837211019488

A review of processing strategies to generate melt-blown nano/microfiber mats for high-efficiency filtration applications

Yahya Kara[1] and Kolos Molnár*[1,2]

1. Budapest University of Technology and Economics, Faculty of Mechanical Engineering, Department of Polymer Engineering, Műegyetem rkp. 3., H-1111 Budapest, Hungary

2. MTA–BME Research Group for Composite Science and Technology, Műegyetem rkp. 3., H-1111 Budapest, Hungary

Corresponding author: Kolos Molnár (molnar@pt.bme.hu)

Abstract

Protective masks – worn properly - have become the key to wither away the COVID-19 pandemic. Nowadays, the vast majority of these masks are made of nonwoven fabrics. High-quality products have mainly melt-blown filtering layers of nano/microfiber. Melt blowing produces very fine synthetic nonwovens from a wide range of polymers and allows a fair control of the fiber structure and morphology that makes it ideal for filtration purposes. Melt blowing has a high throughput, and the low price of the filter makes these products widely available for civil use. Although melt-blown fiber applications were rapidly growing in the last three decades, we still have limited knowledge on the processing parameters. In this regard, we detailed the melt blowing parameters to obtain a filter media with high particle capturing efficiency and a low-pressure drop. We summarized the melt-blown fiber mat characteristics with specific attention to the pore size, the porosity, the fiber diameter, the fiber packing density and the air permeability desired for highly efficient filtration. Even though we cannot estimate the future social effects and the trauma caused by the current pandemic, and protective masks might remain a part of everyday life for a long while. That also implies that near-future investments in wider manufacturing

capacities seem inevitable. This paper also aims to facilitate masks' production with improved filtration efficiency by reviewing the recent developments in melt blowing, the related applications, the effects of processing parameters on the structure and performance of the nonwoven products focusing on the filtration efficiency via knowledge.

Keywords: melt blowing, nonwoven, filter media, fiber structure, respiratory systems, COVID-19

Nomenclature

Notation	Definition	Notation	Definition
MB	melt-blown	PLA	Poly (lactic acid)
ES	electrospun	TPE	Thermoplastic elastomers
NPL	needle-punched layer	PVDF	Polyvinylidene fluoride
MBL	melt-blown layer	PTT	Polytetramethylene terephthalate
SMS	spunbond/melt-blown/spunbond	PMMA	Poly(methyl methacrylate)
NIOSH	the U.S. National Institute for Occupational Safety and Health	PVA	Polyvinyl alcohol
ECS	European Committee for Standardization	PAN	Polyacrylonitrile
COVID-19, SARS-CoV-2	Severe acute respiratory syndrome coronavirus 2	PCL	Polycaprolactone
MFI	melt flow index	PPS	Polyphenylene sulfide
DCD	die-to-collector distance	PDI	polydispersity index
FFP	filtering facepiece	NaCI	sodium chloride
PET	Polyethylene terephthalate	MgSt	Magnesium stearate
PS	Polystyrene	TiO_2	Titanium dioxide
PA	Polyamide	$BaTiO_3$	Barium titanate
PE	Polyethylene	Zeolite imidazole	ZIF
PBT	Poly (butylene terephthalate)	SAP	superabsorbent polymer
PC	Polycarbonate	WAXD	wide-angle X-ray diffraction

PU	Polyurethane	DOP	dioctyl phthalate
PCTFE	Polytrifluorochloroethene	TBC	tributyl citrate
PMP	Polymethylpentene	UV	Ultraviolet
PP	Polypropylene	CV	coefficient of variation

1. Introduction

Melt blowing is a simple, versatile and cost-effective extrusion-based technology that generates continuous nano/microfibers, forming in most cases a randomly oriented web. The fiber mat is formed continuously, the polymer melt is drawn by pressurized hot air. No special additives or binders are required, and there is no need for secondary processes like thermal bonding of the fibers. A variety of additives can be admixed to the base polymer to enhance end properties, similar to any other extrusion-based polymer processing techniques. Melt-blown (MB) fiber mats have high surface area per unit weight, and moderate stiffness and tunable permeability. These properties make them excellent candidates for making high quality filters, surgical drapes and gowns, protective apparel [1-9]. In addition to these, MB nonwovens can also be utilized in a wide range of applications including drug delivery, membrane separation, battery separators, skin and wound dressing and reinforced composite materials [10-16] and they play a crucial role in the fight against the COVID-19 pandemic [17, 18] as the most common filtering media in face masks.

MB fiber mats are formed directly from a molten polymer without controlled stretching. This renders a distinct cost advantage and high production rate in comparison with other micro- and nanofiber generating techniques (*e.g.* electrospinning) [19-23]. Besides, melt blowing is a solvent-free process that makes it economically and environmentally friendly. Moreover, melt blowing is compatible with a broad type of polymers [4]. The properties of the polymer materials have to be optimized to meet the requirements of certain applications. These features may include but not limited to: hydrophobicity/hydrophilicity, piezoelectric or antistatic properties, biocompatibility

or biodegradability, high filtration efficiency or absorbency of liquid matters, possess a high modulus and strength, etc. Often a combination of multiple properties is desired, and that can be achieved with precisely engineered equipment operated within a rather narrow processing window, accurately designed processing parameters, or combination of two or more synthetic materials [24, 25].

The COVID-19 pandemic raised a discussion in both scientific and industrial environments on the high-throughput fine fiber making methods for producing high-efficiency filtering facepiece (FFP) protection and related respiratory systems. Notably, the respiratory devices and related applications of the MB fiber mats are the great interest of both industry and research environments. Melt blowing is often employed in mass production to create such respiratory systems with high quality and high filtration efficiency [26]. Filters made of MB fibers are widely used to capture and filter solid and liquid aerosols[27] and therefore became one of the most essential protective equipment in fighting COVID-19. Respirators made of fiber mats are standardized with different codes (grades) in different countries according to their filtration efficiency. For example, they are represented as N95, N99 and N100 in the USA and KN90, KN95 and KN100 in China [28, 29]. The numbers refer to the minimum filtration efficiency in percent's (90%, 95%, 99% and 99.97%) for a standard aerosol particle size of 0.3 μm (300 nm) [30-32]. In Europe, respirators are coded as FFP1, FFP2 and FFP3 having filtration efficiency of at least 80%, 94% and 99.95%, respectively [33]. Respirators are also designated with N, R, P codes, which stand for not oil resistant, moderately oil resistant, and highly resistant to oil (oil proof), respectively [29]. There are regulations and standards for respirators designation respectively prepared by the U.S. National Institute for Occupational Safety and Health (NIOSH) and by the European Committee for Standardization (ECS) for approval label and related requirements [29, 30, 33, 34]. Approval labels provide essential

information to determine whether a respirator is configured in a manner consistent with conditions determined by the NIOSH and EN 149:2001+A1:2009 and EN 13274-7:2008 and GB 2626-2019 standards. The filtration efficiency ratings of the particulate respirators according to these standards are summarized in Table 1. The allowable breathing resistance (*e.g.*, inhalation and exhalation resistance) is another key feature since it is closely related to the respiratory device's performance and comfort. Therefore, the filter media breathing resistance is standardized according to the graded filtration efficiency. For example, the EN 149:2001 breathing resistance with the inhalation flow of 95 l/min designated 210 Pa, 240 Pa, and 300 Pa for FFP1, FFP2 and FFP3, respectively, while exhalation resistance for all grades limited to 300 Pa with the flow rate of 160 l/min. On the other hand, the GB 2626-2019 standard for disposable facemask (without valve) under the same inhalation and exhalation flow rate of 85 l/min specified the breathing resistance (both inhalation and exhalation) of 170 Pa, 210 Pa and 240 Pa for KN90, KN95 and KN100, respectively. The ECS recently released a guide for face coverings. It is indicated that air permeability must be greater than or equal to 96 l/s/m^2 for a vacuum pressure of 100 Pa [35]. An airborne virus mostly consists of a lipid (fats and oils) sheath; however, the amount of lipid in the virion (floating virus particle) is low; therefore, it does not significantly affect the filtration performance of N series respirators. The actual size of the COVID-19 (SARS-CoV-2) virus is reported around 150 nm, and the $\eta \geq 95\%$ respirators are able to protect against particles in that range[36]. Thus, at least N95, KN95, FFP2 or equivalent respirators are recommended for the protection against the airborne viruses such as the SARS-CoV-2 new coronavirus for those in high risk environments [30, 37].

Table 1. Summary of the particulate respirator efficiency ratings and corresponding standards

	Standard

Particulate respirator efficiency ratings	Description	NIOSH-42CFR84	GB 2626-2019	EN 149:2001+A1:2009
100	captures 99.97 particles out of every 100	N100	KN100	FFP3
99	captures 99 particles out of every 100	N99	KN99	N/A
95	captures 95 particles out of every 100	N95	KN95	FFP2
90	captures 90 particles out of every 100	N90	KN90	FFP1

The high barrier properties against fluids, breathability and efficient particulate and droplet filtration are essential features for the respirators made of nonwovens [38, 39]. The fundamental problem in respiratory filtration systems is ensuring and selecting an appropriate structure of the fiber mats. The filter media is expected to provide high efficiency for various types of conditions [40]. Choosing appropriate processing parameters in generating fiber mats could significantly enhance the end properties of MB fiber mats, hence the filtering properties. Filtration is a complex process that consists of transportation mechanisms and the deposition of particles on the fiber media. In practice, nonwoven filters are expected to have features like low energy consumption of manufacturing, longer service time, mechanical durability, high filtration capacity, easy cleanability and easier maintenance. The filtration efficiency of the MB fiber mats depends on the geometric dimensions of the fibers, thickness, porosity (or packing density) and besides, the nature of the aerosol, the particle size, and environmental conditions such as temperature, relative humidity and air velocity also influence the filtration efficiency [1, 8, 41-43].

Pore size or pore diameter is very important in determining the filtration efficiency of a nonwoven filter. Pore size is directly related to the fiber diameter, the solidity (fiber packing density) and the thickness of the mat. Solidity is the volume of fibers per unit volume of fiber mat,

and it depends on the fiber diameter and geometry within the fibrous structure (*i.e.*, fiber mat). The relationship between pore size, solidity and fiber diameter is given by Eqs 1 and 2 [38, 44].

$$\chi = \frac{V_f}{V_{fm}} = \left(\frac{\frac{m_{fm}}{\rho_{bulk}}}{t_{fm} A_{fm}} \right) = 1 - \varepsilon \tag{1}$$

$$\overline{\mathrm{D}} = \frac{d_f}{\mathrm{g}(\chi)}$$
$$\mathrm{g}(\chi) = \frac{1}{\left[\frac{1}{2(1-\chi)^2 \chi^{1.5} (1+56\chi^3)} \right]^{0.5}} \tag{2}$$

where, χ is the solidity, $V_{fm}$is the volume of the fiber mat (or medium), $V_f$is the volume of the fibers, t_{fm} is the thickness of the fiber mat, d_f is the fiber diameter, ρ_{bulk} is the bulk density of the polymer, m_{fm} is the mass of the fiber mat (or medium), $A_{fm}$is the area of the fiber mat, ε is porosity and $\overline{\mathrm{D}}$ is the average circular capillary-equivalent pore size (derived from the modified Hagen–Poiseuille law).

The fiber mat thickness (*e.g.,* filter depth) and areal density (*i.e.,* surface area per unit mass) are directly related to the filtration performance. Increasing fiber mat thickness and areal density may increase the filtration efficiency. However, this often worsens the filter media properties, such as pressure drop, air permeability, inhalation/exhalation comfort, etc. [38, 45, 46]. Therefore, reducing the fiber diameter and pore size might be a good strategy to adjust the fiber mat thickness and areal density, and so filtration efficiency. Finer the fiber diameter increases the specific surface area, and that in turn gives decreasing pore size [46]. Besides, finer fibers resulted in thinner fiber mat thickness and increases fiber-specific surface area [19]. Decreasing fiber diameter increases fiber-specific surface area, decreases the filter media pressure drop in parallel [47].The pore size also decreases due to the fiber entanglements. With larger diameter fibers, due to their higher bending

stiffness, entanglements will be relatively less. Therefore, generally, nonwovens have no structural barriers restricting their use as filters. The filter pressure drop characteristic is related to the filter thickness, fiber diameter, fiber packing density and filter media's rigidity. However, decreasing fiber diameter results in thinner filter thickness, which might weaken the filter media's mechanical properties [27, 48]. Filter media strength to maintain its structural integrity against the pressure of the fluid flowing through it which is crucial for its operational use.

Although MB fiber mats exhibit high filtration performance, they suffer from weak mechanical properties and poor abrasion resistance. A filter media made of fine fiber (*e.g.,* electrospun or MB) mats are reinforced with external layers to provide structural integrity in facemask applications[49]. These layered structures (*i.e.,* composite) provide density and porosity gradient filtration. Each successive layer provides a high efficiency for capturing smaller particles when the liquid and particle flow through the filter[50]. The SMS (spunbond/melt-blown/spunbond) process and variations are commonly implemented in producing filters due to their good mechanical properties and feasible production on a large-scale[51, 52]. Air permeability is another property which determines the filtration efficiency and quality of the nonwovens. It is defined as the rate of airflow passing perpendicularly through a known area of the filter under a certain pressure difference between the two sides of the filter [53]. It provides a measure of nonwoven porosity and relates directly to its thickness and density. Low air permeability filter media are desired for efficient filtration considering particle capturing in the air more effectively. However, too low air permeability is not favorable for air filter media, because it reduces the inhalation and exhalation quality and people wear the mask less-likely. On the other hand, higher air permeability gives, in turn, better breathability. When the air permeability is high, the exhaled air might go through filter media smoothly, and the user comfort will be better in terms of inhalation and exhalation. The

COVID-19 outbreak revealed that the user's comfort related to air permeability is one of the biggest challenges in making face masks (*e.g.* N95, KN95, FFP3) made of MB fiber mats. Therefore, air permeability in terms of filtration application needs a systematic optimization for high-quality filter media. Despite the higher air permeability render a good barrier property of fiber mats, it is not favorable for applications such as respiratory devices since it reduces filtration efficiency.

There is a close relationship between the pore diameter, the fiber diameter and the air permeability, which are crucial for filtration efficiency [54, 55]. However, these properties do not go hand in hand, one has to compromise to get the parameters close to the desired. However, high bulk density and air high permeability with the smallest pore sizes are expected for highly efficient nonwoven filters. Smaller fibers yield small pore size and high filtration efficiency. On the other hand, larger fibers might provide bulky media and improved permeability, but that could, in turn, give a significant loss in filtration efficiency [3].

Up to date, a massive effort has been dedicated to fundamentally understand and to improve the filtration efficiency of MB fiber mats and the fiber formation process itself. In the present study, we aim to detail the current scientific and technological advances in melt blowing, and MB fibers used in filtration applications. Our other goal is to develop an overall and more in-depth understanding of the relationships of the melt blowing process, the structure and the filtration performance.

2. Melt Blowing Process and Related Polymeric Materials

In melt blowing, the polymer melt is extruded through a die containing numerous small capillaries then stretched via a jet of hot air. The ratio of high velocity air versus the lower velocity polymer provides a drag force that rapidly attenuates the forming fibers. Then, the fibers are

collected on the surface of a collector in the form of a random web. The method was first developed in the 1950s at the U.S. Naval Research Laboratory by Wente with the goal of making sub-micron fibers to trap radioactive particles in the upper atmosphere [56]. Wente was able to generate polyamide and polyester fibers with a diameter of less than 1 micron and as thin as 100 nanometers by hot air steam. The concept of Wente is consisted of a ram extruder that forced a molten polymer through a row of capillary holes directly into high velocity heated air. The fibers formed through the gas steam when cooler ambient air solidified the molten polymer towards the collector. This concept was quite similar to the manufacturing of mineral wool patented by John Player [57] in 1870. The patented process involved blowing a strong stream of air across a falling flow of liquid iron slag. When a powerful blast of steam met the liquid slag, that separated the melt into long filaments. The industrialization of a similar method was carried out by another patent by Charles Corydon Hall [58] in 1902 to produce a highly porous mineral-wool felt. The idea of applying hot air steam for fiber generation had been followed by another patent authored by John H. Thomas of the Owens-Corning Fiberglass Corporation [59] in 1940 to manufacture glass wools. After the first steps of Wente in the 50's, today's well-known companies like DuPont [60], Exxon [61], Kimberly-Clark [62], Johnson & Johnson [63], 3M [64] and many others [65-68] took an active part in developments and industrialization of melt blowing and MB fibers in the subsequent years [69]. Wente reported nanofibers of PET, PA6 and PA6/10 polymers with an average diameter of 500 nm achieved the production rates of 0.54 – 1.62 kg/h/m of die width. Later on, a 36-inch-wide (914 mm) die based on this concept was developed by Exxon Company [70]. Exxon was able to improve the technology to commercially attractive throughput rates of 2.15 – 40 kg/h/m of die width [71]. Nowadays, Reicofil Reifenhauser provides multi-row melt blowing lines having 12,000 nozzles per meter and fibers ranging from 1-25 microns and a throughput rate up to 150 kg/h/m [72]. Among the other methods

like electrospinning, melt blowing is now one of the fastest growing, high throughput and most modern methods of manufacturing of sub-micron and nano fiber mats. A typical melt blowing setup (**Figure 1**) consists of four main parts, which are: an extruder, melt blowing die head, hot air feed and a collector that comprises a drum, continuous band or a fixed part.

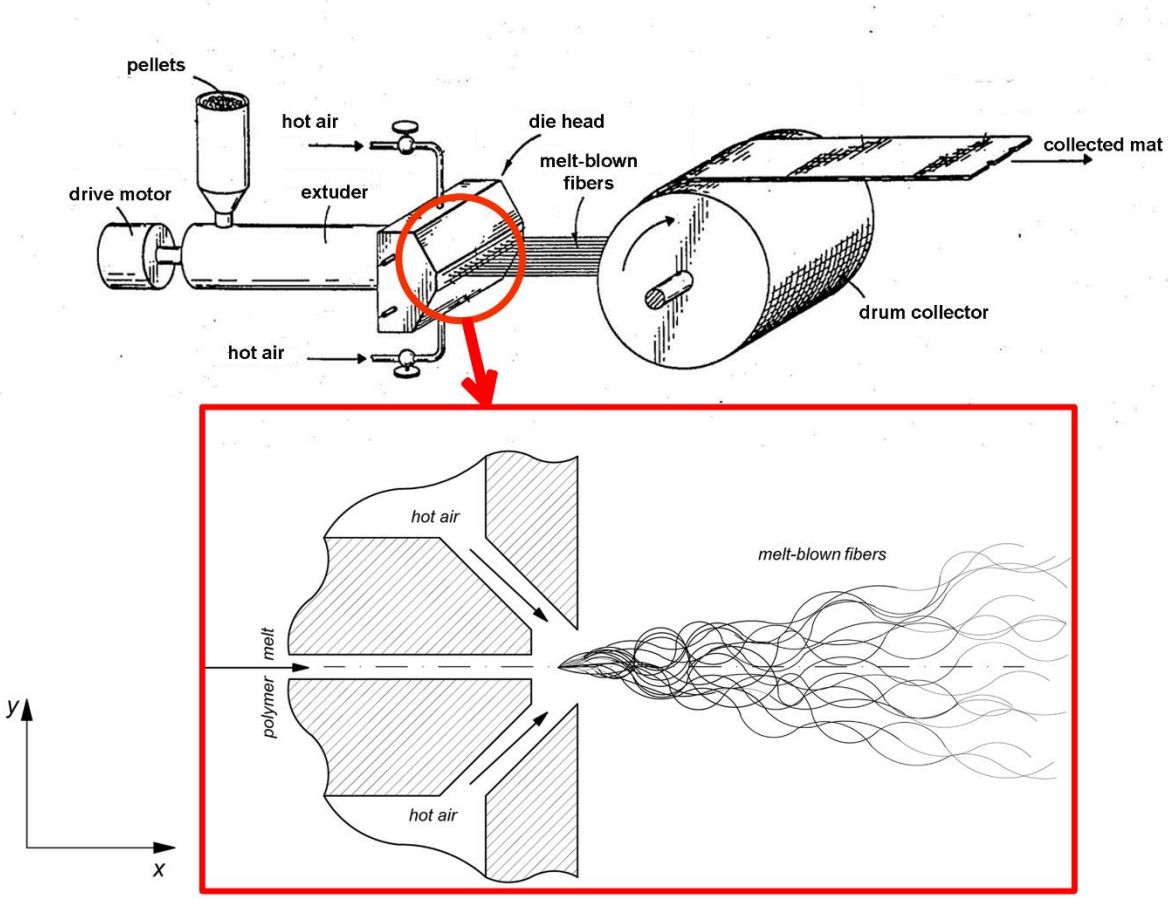

Figure 1. Schematic of a typical melt blowing system [73] and illustration of the melt blowing fiber formation at the die

A broad range of polymers and polymer blends are compatible with melt blowing. In order to obtain MB fibers, the molecular weight (M_w) associated with the melt flow index (*MFI*) [g/10 min] needs to be proper. The most common polymers for melt blowing are polyolefins (especially PP) due to their physical properties, ease of processing, low cost and versatility in making a wide range

of products. Polymers commonly used to produce micro/nano fibers by using MB technology are given in Table 2 with details.

Table 2. A summary of polymers and corresponding fiber diameter, melt flow index and melt temperature utilized in the melt blowing technology

Polymer	Average fiber diameter [μm]	MFI ASTM D1238 (viscosity)	Melt temperature [°C]	Reference
Polypropylene (PP)	0.3	1500	220	[74]
Polyphenylene sulfide (PPS)	4.1	-	-	[75]
Polyethylene terephthalate (PET)	5	375	315	[76, 77]
Polystyrene (PS)	0.38	(1.1) *	280	[74]
Polyamide (PA) (6, 66, 11, 12)	0.8	-	-	[56]
Polyethylene (LDPE, HDPE)	<12	155	255	[19]
Poly (butylene terephthalate) (PBT)	0.44	250	265	[74]
Polycarbonate (PC)	1.1	15.4	370	[78]
Polyurethane (PU)	4	-	230	[79]
Polytrifluorochloroethene (PCTFE)	2	~600	254	[80]
Polymethylpentene (PMP)	3	3000	255	[81]
Poly (lactic acid) (PLA)	0.4	77.5	244	[82]
Thermoplastic elastomers (TPE)	5	25	285	[83]
Polyvinylidene fluoride (PVDF)	<3	1200	-	[84]
Polytetramethylene terephthalate (PTT)	1.7	385	288	[85]
Polyesteramide (PEA)	10.2	21	230	[86]
Poly(methyl methacrylate) (PMMA)	1.5	-	-	[56]

*Pa.s (measured at 280°C, zero shear rate)

In general, a low M_w corresponding to a low viscosity and a high MFI is desired, because it can lower the processing temperature and thus decrease the manufacturing cost. The low viscosity and

high MFI provide a more uniform web with thinner fibers in the melt blowing process due to higher attenuation applied through hot air steam. In the literature, it is suggested that the suitable range of MFI for polymers used in melt blowing is 15-3,000 g/10 min [4, 56, 87, 88] as a rule of a thumb. The high polymer viscosity and i.e. low MFI yields formation of larger fibers; hence, the advantage of the process in forming ultra-fine fibers is lost [87]. Besides, the average M_w and the narrow molecular weight distribution is important to obtain MB fibers. The melt flow rate of the polymeric resins depends upon the molecular weight and its distribution. The narrower molecular weight distribution renders a high melt flow rate. Lower viscosity is an essential requirement of the polymeric resins used in melt blowing. A narrow molecular weight distribution reduces the melt elasticity and melt strength of the polymer so that the melt stream can be drawn into fine fibers without excessive draw force [88, 89]. However, a wide molecular weight distribution increases melt elasticity and melt strength and result in fiber breaks and flaws due to melt instabilities [4, 74]. The decrease in elongation causes the increase in fiber diameter and fewer fiber entanglements. Tan *et. al.* [90] reported that increasing melt elasticity increased the fiber diameter and decreased the coefficient of variation (CV) (also known as normalized width of the fiber diameter distribution) while increasing viscosity did not significantly affect the CV. Drabek and Zatloukal [91] reported that polymer molecules chain branching could lower the CV of fiber diameter distribution, while they stated chain branching did not significantly influence the average fiber diameter. In general, decreasing molecular weight or increasing melt temperature increases (e.g., due to the decreasing reptation-mode relaxation time) the CV of fiber diameter distribution. They also found that the CV of fiber diameter distribution significantly decreases due to the extensional strain hardening at the post die zone [92]. They stated that increased strain hardening in uniaxial extension at post die zone

could withstand inhomogeneous stretching in the post-die area, which reduces CV of fiber diameter distribution.

A measure of the breadth of the molecular weight distribution is given by the ratios of molecular weight and number mass averages ($\frac{M_w}{M_n}$), called the polydispersity index (PDI). Jones [93] studied the influence of polydispersity on the mechanical characteristics of polypropylene (PP) MB webs. The mechanical properties of PP MB webs are slightly affected by the changes in PDI. The strength of web decreases with the increasing degrees of PDI.

3. Processing Parameters Affecting the Fiber Mat Characteristics and Filtration Efficiency

Considering engineering and medical applications, MB fiber mats provide advantages of high filtration efficiency and low air resistance besides many other advantages [6, 94, 95]. Thanks to the very high surface area to volume ratio, highly porous structure with moderate mechanical strength, and the high surface cohesion, the MB fiber mat filters can capture tiny particles less than a micron. Moreover, the filtration efficiency can be improved further with optimizing processing parameters based on the requirements that can go up to less than 0.3 μm.

The filtration efficiency of the MB fiber mats highly depends on the processing parameters which directly relates the structure (*e.g.,* fineness and evenness), pore size, strength, fiber diameter, thickness (packing density) and the air permeability (resistance) across the filter. The diameters of polymeric fibers can be drawn in the high-speed hot air in the range from nanometers to micrometers if appropriate parameters of the process are maintained. The MB fibers are susceptible to the processing parameters set, and they can either improve or drop the nonwoven

characteristics. Therefore, examining the suitable processing parameters is necessary for the MB fiber mat to fulfill the requirements of the related application field.

3.1. Polymer throughput rate

The polymer flow rate plays key roles in the resulting diameters of MB fibers. The polymer flow rate (throughput) at a given setup can be increased by increasing the extruder screw speed. Increasing polymer throughput rate while keeping the other processing conditions unchanged results in an increase in the average fiber diameter [96]. It is because the same drag force from the air jet acts on a higher polymer mass. In general, increasing polymer flow rate can increase the fiber diameter and that in turn gives a coarser fiber morphology and decrease of quality of the MB fiber mat. Zhang *et. al.* [97] found that increasing polymer throughput rate from 03 g/h/m to 1.5 g/h/m increased the Poly (trimethylene terephthalate) (PTT) MB fiber diameter around 20%.

Xu and Wang [95] reported that air permeability, fiber diameter, area density and surface density unevenness of PP fiber mats increases with increasing the polymer throughput rate. They stated that increase in the air permeability is due to the increased fiber diameter and it leads to big pore sizes between the fibers, therefore it results in a good air permeability of the PP fiber mats. Typically for MB fiber mats with all the other conditions being same, increasing polymer throughput rate tends to increase fiber diameter and obviously the areal density. Increasing the throughput rate causes broader fiber diameter distributions and a coarse fiber morphology (*e.g.* defect formation, larger pores and larger basis weight), which is unfavorable [98, 99]. Guo et. al.[100] demonstrated that increasing polymer throughput rate increases PP (MFI= 1200 g/10 min @230 °C, 2.16 kg) fiber diameter from 3 to 10.5 µm while porosity and surface are decreases from 90% to 75% and 1.5 m^2/g to 0.5 m^2/g (**Figure 2**).

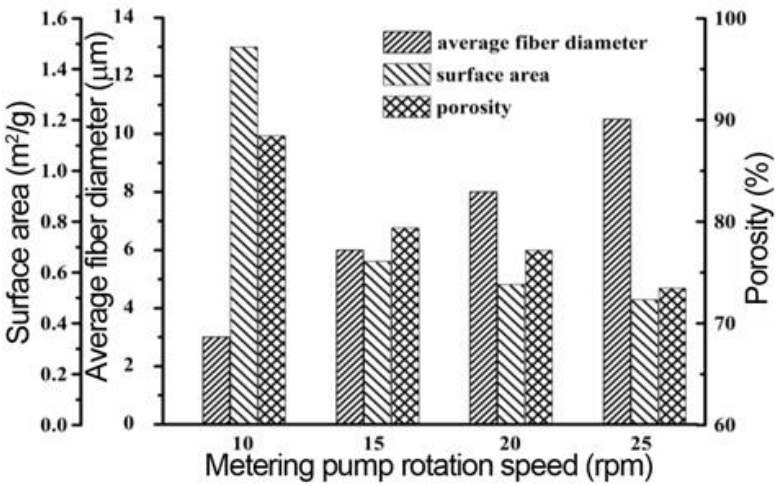

Figure 2. Influence of polymer throughput rate on PP fiber mat porosity and surface area and average fiber diameter [100]

Marla and Shambaugh [101] concluded that lower polymer flow rates results in smaller fibers that causes the rapid cooling of MB isotactic polypropylene (iPP) fibers (MFI= 88 g/10 min @230 °C, 2.16 kg). It is because of the lower thermal inertia of the thinner fibers increases the cooling rate. On the other hand, a lower polymer feed rate provides longer residence time in the extruder, which might cause the thermal degradation of the polymer. Nevertheless, various research groups reported that a decrease in the polymer flow rate leads to obtaining thinner fibers [96, 102]

3.2. Air Pressure (Air flow rate or Air velocity)

Air pressure and air velocity, which are related to the air flow rate, influence the morphology. In melt blowing, a higher air velocity results in a higher attenuation and a smaller fiber diameter. The compressed hot air used in melt blowing was revealed to be the major energy cost. Using very high air velocity might result in a fiber break up and short, fragmented fibers. And this defect is often called fly. It occurs because of the strong cooling effect on the thinned fibers [81]. In contrary, at too low air velocities, the polymer mostly would not form a fibrous mat but would fuse into a film-like body on the collector [103]. The increase of the air velocity, usually achieved by increasing

the air pressure, can break up fibers and generate fiber loose. It was reported that such instabilities cause the fiber jet break by the increase of air pressure. [74]. Drabek and Zatloukal[104] summarized these flow instabilities and defect formation mechanisms at the melt blowing process. We refer the reader to their study for an in-depth understanding of such phenomenon, including whipping, die drool, onset fiber breakup, melt spraying, flies, shots, jam, etc.

Yeşil [105] reported that increasing air pressure decreases the basis weight and air permeability of TPU MB fiber mats (**Figure 3** (a)-(b)). Decreasing basis weight can be associated with the reduced fiber diameter with increased air drawing rate. In general, the lower air permeability translates to higher filtration efficiency, which means less particle and fluid to pass through the filtering media. Besides, he reported that tear strength decreased with increasing air pressure (**Figure 3** (c)) due to the air quenching, which reduces fiber to fiber bond strength.

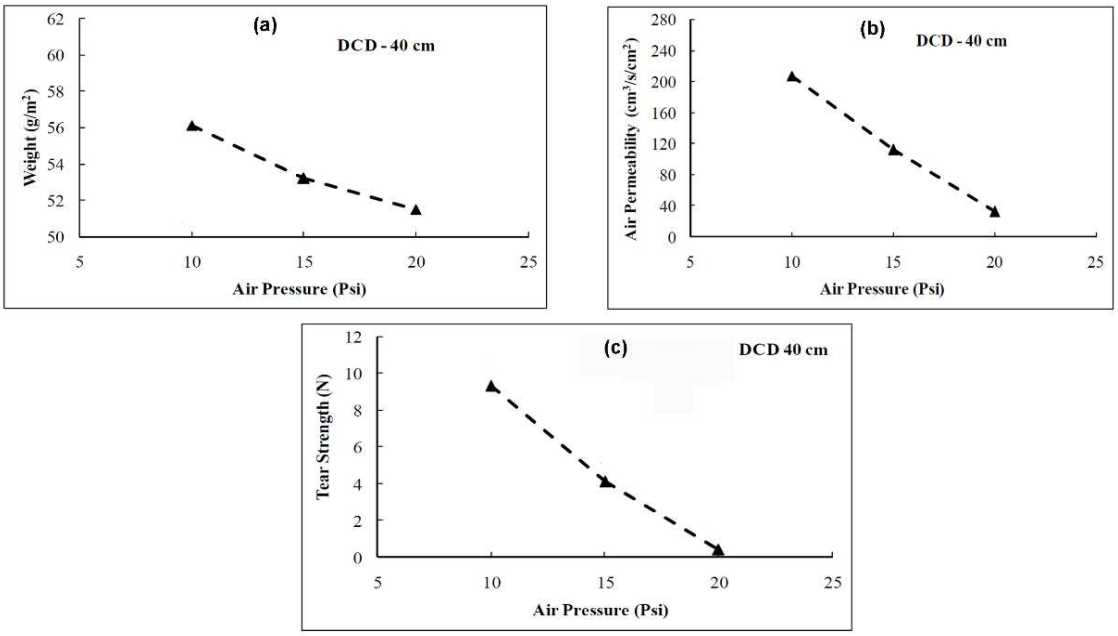

Figure 3. Effect of air pressure on the MB fiber mat (a) basis weight, (b) air permeability and (c) tear strength (DCD: die-to-collector distance)[105]

Milligan and Haynes [106] worked on melt blowing of a different types of PP (MFI varied between 500-900 g/10 min @230 °C, 2.16 kg). They reported that a ratio of air to polymer mass fluxes (Γ) provides an approximate description of the fiber size for a wide range of processing conditions (Eqs. 3). They found that increasing Γ results in a decrease in the average fiber diameter of the MB fiber, as shown in **Figure 4.**

$$\Gamma = \frac{\dot{Q}_a / A_{ae}}{\dot{Q}_p / A_{pe}} \tag{3}$$

where, $\dot{Q}_a$ is the air flow rate [m^3/s], A_{ae} is the air outlet area [m^2], $\dot{Q}_p$ is the polymer flow rate [m^3/s] and A_{pe} is the polymer melt outlet area [m^2]. On the other hand, increasing Γ broadens the fiber diameter distribution's CV due to the increase in the turbulence of the air flow field. But, the fluctuation of air flow (turbulence) can decrease the evenness of the MB fiber mat [107].

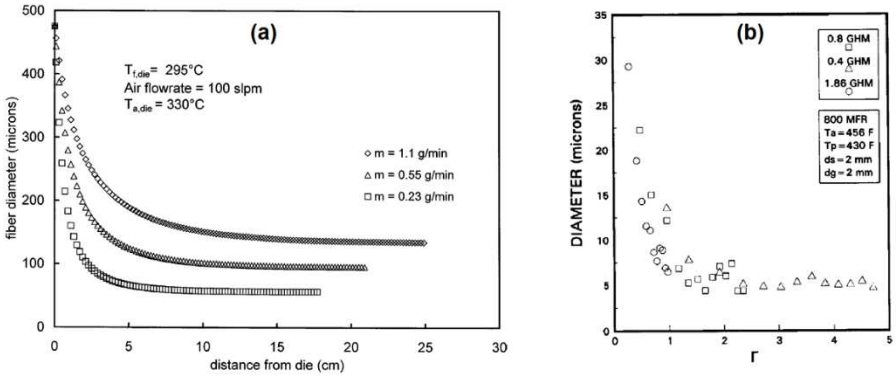

Figure 4. (a) The effect of polymer flow rate on fiber attenuation [101]and (b) the average fiber diameter versus air to mass ratio for three throughputs [106]

Higher air velocity attenuates the fibers more since the air exerts a higher forwarding drag force on the fibers. Uppal *et al.* [108] reported that the average diameter of the PP fibers produced by melt

blowing pilot line reduced by about 70 nm (from 590 nm to 520 nm) with the increase of air flow pressure from 70 to 140 kPa in the case of the die used. Milligan *et al*. [109] worked on the influence of an additional unheated air flow namely crossflow on the MB fiber morphology. They used two crossflow chambers placed parallel next to the melt blowing die. In their study, the influence of various crossflow angle, which is between spinline and slit (*e.g.*,45°, 20°, 10°), were investigated. They concluded that applying a crossflow can decrease the average fiber diameter of MB hPP (MFI= 800 g/10 min @230 °C, 2.16 kg) fibers around 45% (from ~11 μm to ~6 μm) when the slit angle was 20°. Xie *et al*. [107] concluded that the air velocity attenuates the fibers in their molten state. Otherwise, there is no contribution of high air velocity to fiber attenuation after the fiber solidified. Therefore, the further increase in air velocity can cool the fiber faster and hence, the attenuation process slows.

However, higher air pressure can translate air flow regime from laminar to turbulence, and further increasing air velocity could increase the CV of fiber diameter, which is unfavorable [110, 111]. Tan *et. al*. [90] reported that increasing airflow rate from ~147 l/min to ~272 l/min increased the CV of fiber diameter from 10% to 20% while the fiber diameter decreased around 40%. Choi *et al*. [112] found that the stiffness of the different grade homopolypropylene (hPP) (MFI= 300-35-12.7 g/10 min @230 °C, 2.16 kg) MB fiber webs decreased as the air pressure increased. They also reported that increase in the air pressure causes a reduction in both fiber diameter and inter filament (fiber fuse) bonding.

The hydrostatic head is another factor: the measure of fiber mat resistance against the liquid pressure. When the fiber mat hydrostatic head is high, it translates to a greater barrier to liquid penetration. With this regard, a high hydrostatic head means small pores and thin fibers in the fiber mat structure, indicating favorable physical properties. Yesil and Bhat[39] found that when the air

pressure is increased from 20 to 35 kPa, the mean flow pore diameter and air permeability decrease, and they reported the reduction could be attributed to the fiber diameter (**Figure 5**) that also decreases with increasing air pressure. However, they did not find a significant change in air permeability and mean pore diameter for the further increase in air pressure. In addition to these, increasing air pressure from 20 to 35 kPa resulted in the increasing of the hydrostatic head of fiber mats in a range between 54 and 97%. And they reported a slight decrease in the hydrostatic head with a further increase in air pressure. Decrease in the average pore size translates the increasing resistance of the fiber mat against fluids, so the penetration or passing of the fluid through the fiber mat media becomes hindered. As a result, the hydrostatic head of the fiber mat was increased.

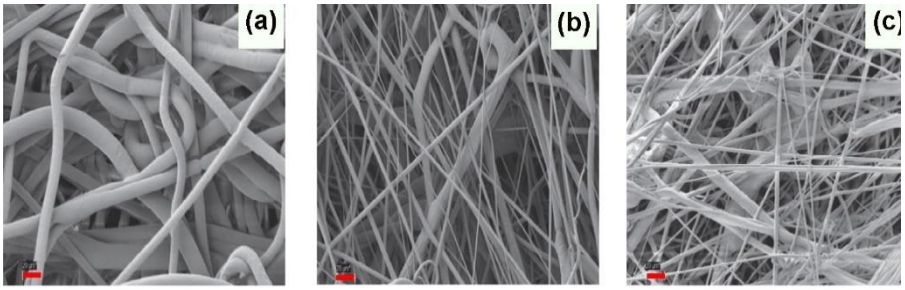

Figure 5. SEM images of PE MB fiber mats produced at various air pressure; (a) 20 kPa, (b) 35 kPa, (c) 70 kPa (red-colored scale bars on the bottom left of the figures represent 20 μm) [5]

Bresee *et. al.* [113] reported that increasing air pressure reduces the size and the number of pores in MB fiber mats. Increasing air velocity also reduces the aspect ratio of pores. The reduction in pore size is attributed to the decrease in fiber entanglements and to the reduced fiber diameter as the airflow increases. Hammonds *et. al.* [82] studied the influence of air flow rate (*i.e.* air pressure) and DCD on the pore size distribution of the PLA MB micro and nano fiber mats. They found that increasing air flow rate and decreasing the DCD reduced the pore size of PLA fiber mat as shown in **Figure 6**. They also reported that the tensile strength of the PLA microfiber and nanofiber mats

increased with increasing airflow. Increased tensile strength of the PLA fiber mat is associated with the preferred molecular orientation by large air attenuation and fiber orientation onto the collector.

In general, MB fiber mat thickness decreases with increasing air pressure. A decrease in fiber diameter with increasing air pressure results in longer collection times in order to achieve the same basis weight. Long collection time translates more fibers and so thicker layers. With increasing air pressure, this phenomenon causes decreasing mat thickness and makes smaller pores with higher packing density [1, 82].

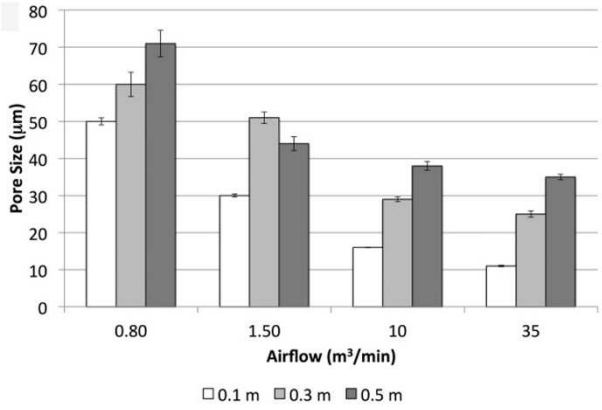

Figure 6. Variation of the mean pore size with respect to air flow rate and DCD [82]

Tyagi and Shambaugh [114] studied oscillating (whipping) air jets to produce PP (MFI = 75 g/10 min @230 °C, 2.16 kg) fibers by melt blowing. They found that oscillating air jets resulted in finer fibers than those produced by using the classical, steady air jets. The attenuation of molten fiber jets in supersonic airflow created by a de Laval nozzle is effective for fine fiber production via melt blowing [107]. Tan *et al.* [115] studied the effect of increasing inlet air pressure in the melt blowing die and the effect of a de Laval nozzle attached to the die face. Increasing air inlet pressure leads to a transition from subsonic to the supersonic flow at inlet pressures greater than approximately 1 bar. However, they observed that the de Laval nozzle's use suppresses compression waves

sourced by the unstable airflow field that causes defect formation (e.g. fly) up to certain air pressure. The corresponding centerline air velocity increases with increasing air pressure until reaching supersonic flow where the fiber spinline begins to oscillate. This phenomenon can lead to defects and probably significant whipping of the fiber jet. Violent vibrations can cause fiber breakage, shots and sticking [74]. However, Xie *et al.* [116] reported that the spiral path of whipping close to the die plays an important role in fiber attenuation. In general, increasing the air velocity can reduce the average MB fiber diameter. But it has not been favored by industries since it significantly increases the cost of production.

The air pressure controls the fiber attenuation mechanism, the entanglements, the uniformity and also influences the defects of the fiber mats [117]. Besides, the higher air velocity can lead to faster cooling of the forming fibers. A slight decrease in the crystalline fraction of the MB fibers is expected in the case of semi-crystalline polymers due to the rapid cooling of the polymeric fibers as a nature of the melt blowing techniques [76, 118]. Higher air pressures were mostly suggested in the literature to achieve thinner fibers. However, air pressure has to be carefully controlled since higher air velocity can cause breakage of the spin-line and result in shot, fly imperfection and relatively larger fiber diameters due to fiber fuse [119].

3.3.The Effect of Melt and Air Temperature

Increasing air temperature and melt temperature leads to a reduced polymer viscosity which increases the attenuation. The air drag generates a higher stretching on the polymer between the processing temperature and the solidification temperature (crystallization temperature for semi-crystalline polymers that are typically used at melt blowing). In general, the higher temperatures are not favorable in melt blowing with respect to the degradation of the polymer. In this regard, Drabek *et. al.*[120] reported that an hour of residence time at the processing temperature (combined

with medium high shear rate level) resulted in nearly 40% decrease in the PP resin's (MFI = 1200 g/10 min at 230 °C, 2.16 kg) molecular weight due to chain scission. Lee and Wadsworth [121] demonstrated that increasing the air temperature from roughly 210 °C to 240 °C led to a nearly 50% reduction in the average fiber diameter of iPP (MFI = 700 g/10 min @230 °C, 2.16 kg), where the smallest fiber diameter they obtained was around 5 μm.

Bansal and Shambaugh [102] carried out a series of melt blowing experiments of PP (MFI = 75 g/10 min @230 °C, 2.16 kg) at different air temperatures with an experimental melt blowing slot die. Their results show that increasing the air temperature causes an increase in the attenuation rate of the fiber and produces a finer fiber (71.7 μm → 62.5 μm) as shown in **Figure 7**. Guo *et. al.* [100] investigated the relationship between the melt blowing process parameters and the PP fiber mat structure. They reported that the porosity of the PP fiber mat did not change with increasing air temperature from 300 to 330 °C in spite of the finding that increasing air temperature resulted in decreasing the average fiber diameter. On the other hand, Xie *et al.* [107, 122] reported that higher air temperature does not always produce fine fibers with even diameter distribution. They obtained that increasing temperature might cause thicker fibers and defect formation due to the turbulent flow by increasing air temperature. Besides, the air cools down very fast when it exits the die due to the low ambient temperature. This effect depends on the polymer melting temperature and the air-fiber temperature gradient towards the collector. Air temperature usually just slightly influences fiber morphology for high DCDs, in many cases its effect on the fiber diameter is negligible.

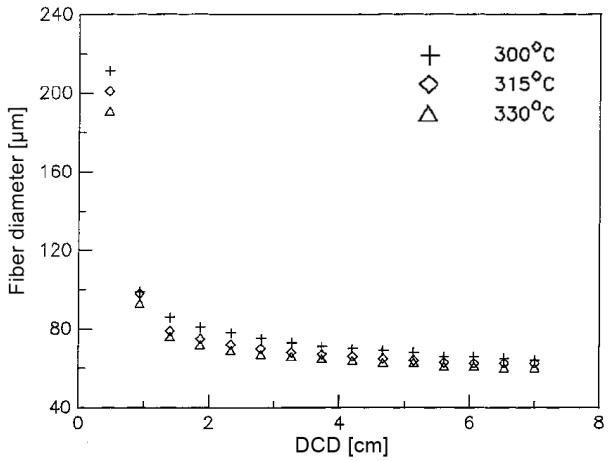

Figure 7. Change in fiber diameter as a function of DCD with air temperatures between 315-330 °C [102]

Moore *et al.* [123] reported that the temperature of the melt blowing die (and therefore the melt) plays a crucial role in the fiber attenuation and affects the fiber diameters and pore sizes significantly. They found that increasing the die temperature from 250 °C to 300 °C decreases the average fiber diameter of the MB fibers around 50% (from 12 to 6 μm). On the other hand, Marla and Shambaugh [101] reported that the further increase in polymer temperature would result only in a slight decrease in the fiber diameter.

Yesil and Bhat [5] studied the influence of the die temperature on PE (MFI = 155 g/10 min @190 °C, 2.16 kg) fiber mat's porosity and barrier properties. They reported that the mean pore diameter of the MB fiber mats produced at 255 °C is slightly lower (~15%) than those processed at 240 °C. However, they found that the effect of the die temperature on the air permeability is negligible. In the same study, the hydrostatic head of PE fiber mat increased by increasing the die temperature. The higher die temperatures not only result in smaller pore diameter and higher hydrostatic head, but also finer fibers were obtained. However, Xu and Wang [95] reported that in the case of PP, increasing air temperature from 170 °C to 230 °C decreases air permeability from 1054 mm/s to

689 mm/s. This improvement is attributed to that finer fibers were produced at higher temperatures. During melt blowing non-isothermal crystallization occurs due to the large temperature difference between the die and ambient temperature. Lower crystallinity is expected due to rapid cooling, which causes reduced polymer chain segment motions. Therefore, the collected MB fibers exhibit relatively low crystallinity due to the effect of quenching [82].

There are no reports on achieving greatly thinner fibers by simply increasing polymer or air temperature which is possibly because of the risk that high temperature is likely to cause thermal degradation. Nevertheless, the high temperatures can be considered for producing fine fibers as long as the extra production expenses are acceptable, and there is no oxidation of the polymer occur and no defect formed *e.g.,* fiber fuse, fiber breakage, shot, fly, etc.

3.4.The Effect of Die-to-Collector Distance (DCD)

The die-to-collector distance (DCD) influences the fiber diameters since it correlates with the dwell time of the fiber attenuation. This results in changes in both the aerodynamic drag and fiber-fiber entanglements and their fused bonds. Besides, as fiber jet travels along the collector the molecules become oriented [124]. The typical DCD at melt blowing is in between 50 - 500 mm.

The DCD can have various effects depending on the material due to the intrinsic properties, *i.e.* crystallization behavior, molecular weight, relaxation time, etc. The average diameter of the fibers produced at a greater DCD tends to decrease due to the more time of the attenuation as shown in Figure 8 [106, 119, 121, 122].

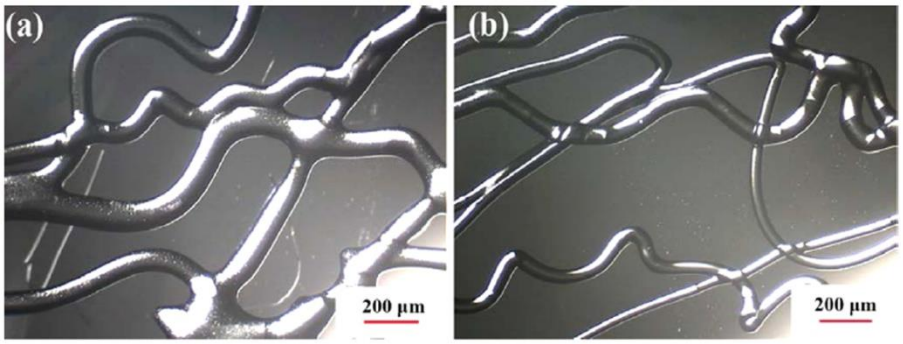

Figure 8. Optical microscopic images of PP MB fibers produced at (a) DCD = 25 mm and (b) DCD = 50 mm [122]

Increasing DCD translates the fibers travel longer distances, and that might result in an altered crystallization kinetics, *e.g.* change in the degree of crystallinity. However, higher DCDs may result in diminished interfiber adhesion and web strength originating from the lower fiber contact temperatures [125]. Feng [126] reported that increasing DCD decreases the PLA fiber mat web strength despite the thinner fiber produced at larger DCDs as shown in **Figure 9**. Yesil and Bhat [19] reported increasing DCD resulted in a looser web structure and so poor mechanical properties due to reduced fiber entanglement.

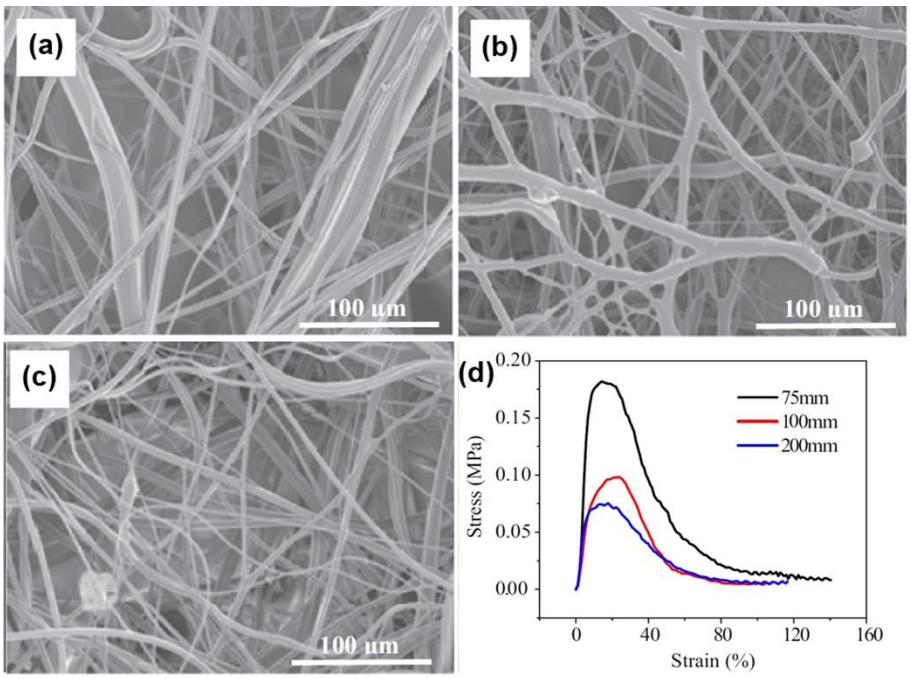

Figure 9. SEM images at DCD of (a) 75mm, (b),100mm (c) 200mm and (d) stress–strain curve of the PLA fiber mats collected at various DCDs [126]

Increasing DCD results in fiber collection over a wider area. It also results in a softer, fluffier structure, so increasing DCD decreased fiber mat solidity [95, 127]. The effect of the increased deposition area is smaller than the effect of decreased fiber mat solidity and that results in a thicker fiber mat. The mat thickness correlates to the packing density, which is a crucial factor in determining the pore size. Denser fiber packing can be reached with a thicker layer of fibers that will result in higher efficiency of the filter [42, 128] with an increased pressure drop. Therefore, the mat thickness and packing density has to be optimized and DCD is the key parameter in that. Slightly finer fibers at higher DCD can be obtained due to the deformation of hot uncrystallized fibers [108]. Chen *et al.* [129] obtained that PBT (MFI = 62 g/10 min @ 250°C, 2.16 kg) fiber diameter decreases 13% as the DCD increase from 100 to 140 mm. However, they reported that the fiber diameter only decreases slightly when the DCD is larger than that. Uppal *et. al.* [108] generated MB

PP fibers and investigated the influence of relatively large DCD (250 mm to 350 mm) on the fiber mat characteristics. They produced PP fiber mat samples with the same basis weight (~25 g/m^2) while the mat thickness increased from 0.44 mm to 0.53 mm with increasing DCD. They found that the pore diameter decreases from 10.4 μm to 6.5 μm with an increase of DCD from 250 to 350 mm while the fiber diameter and air permeability of the fiber mats decrease slightly. The reduced pore size is related to a higher degree of fiber entanglement. This is because of the improved self-bonding of the thinner and continuous MB fibers produced for the same basis weight. As a consequence, the resistance to the penetration of liquid through the MB fiber filter media increases, and that in turn increases hydrodynamic head as shown in **Figure 10**. The pressure drop of the filter media first increased from 49 Pa to 55 Pa with increasing DCD then it became constant due to reduced pore size. However, the filtration efficiency is slightly improved from 80% to 82% due to the smaller pore size as well as greater specific surface area of the finer fibers produced at higher DCD. The slight increase of these properties indicates smaller pores, greater specific surface area of the thin and continuous fibers and higher degree of fiber entanglements.

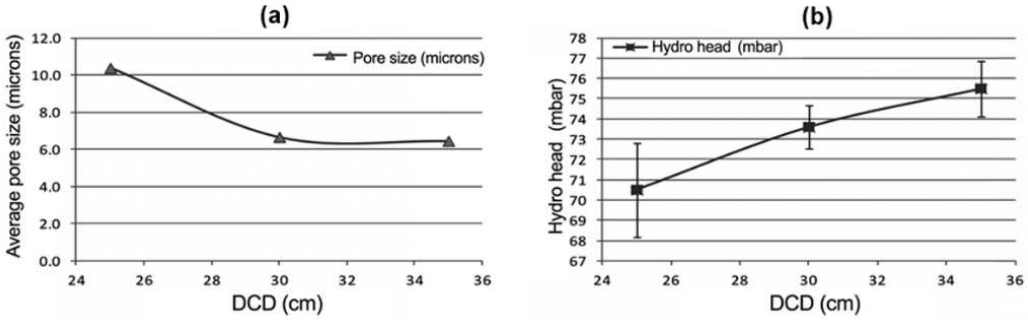

Figure 10. Influence of DCD on the PP web (a) pore size and (b) hydrostatic head characteristics [108]

Choi *et al.* [112] reported that increasing DCD improves tenacity and decreases Young's modulus of hPP (MFI= 300-35-12.7 g/10 min @230 °C, 2.16 kg) fiber mats and results in increased

elongation at break. Besides, they found that an increase in DCD reduces the bonding of the fibers (fuses) without much effect on the fiber diameter. Bresee and Qureshi [130] studied the effect of DCD on the diameter MB PP (MFI = 1,259 g/10 min @230 °C, 2.16 kg) fibers with commercial and experimental melt blowing lines. They found that the average fiber diameter decreases with the increase of DCD, but the influence is very weak. The average fiber diameter reduced by nearly 11% for the experimental line and 15 % for the commercial line with 600 mm increase of DCD from 200 to 800 mm. They also stated that the maximum fiber diameter and its CV increase with the increase of DCD due to the fusion of fibers.

In another study, Bo [131] reported that upon increasing DCD the diameter of PP (MFI = 34.2 g/10 min @ 230°C, 2.16 kg) fibers first decreases and the attenuation stops in a certain DCD and the diameters starts increasing again (**Figure 11**). He stated that after this point, long time travelled fibers begin severely entangled and stick to each other and that in turn gives an increase in fiber diameter and uneven structure for very long DCDs (above 1000 mm).

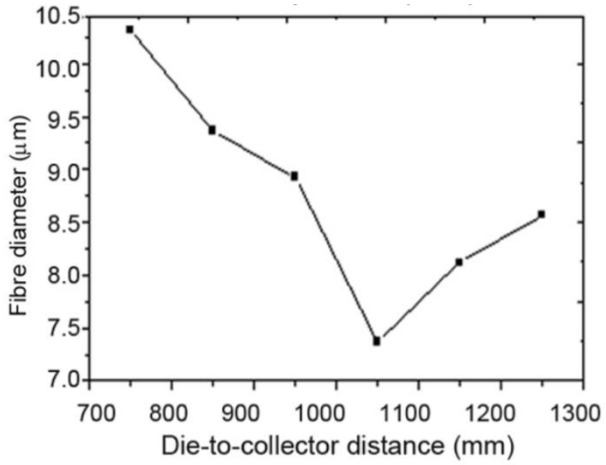

Figure 11. Change in fiber diameter respect to very high DCDs [119]

Lee and Wadsworth [121] studied the influence of processing parameters on melt blowing of iPP (MFI = 700 g/10 min @ 230°C, 2.16 kg). They reported that decreasing DCD increases the degree of fiber entanglements but does not affect the average fiber diameter. On the other hand, as the DCD increases the fibers are laid down with less air drag force and the effect of air pressure is reduced. Also, air turbulence is high at the collector drum and longer DCDs allow the fibers to be laid down over a wider area as shown in **Figure 12** [127]. In the case of polyolefin polymer fibers like PP, lower DCD results in less time for fibers to contact each other. So, fibers become less entangled before reaching the collector. In addition to this, decreasing DCD results in increasing fiber separation in a high air flow and could turn in reducing the number of fiber entanglements [127].

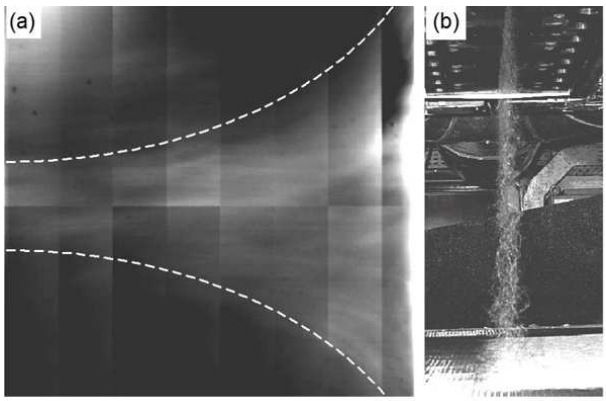

Figure 12. Fiber flow in (a) horizontal (drum collector) and (b) vertical (flat conveyor belt) melt blowing line [132]

Peng *et al.* [133], reported that increasing DCD resulted in an increase of the average diameter of MB PP (MFI = 800 g/10 min @230°C, 2.16 kg) and PP/TPU (MFI = 73 g/10 min @230°C, 2.16 kg) fibers and decreases the CV. They also found that the elastic recovery rate and bulkiness (solidity or fiber packing density) increase and softness decreases, while DCD increases. Another

research group reported a similar result on MB TPU fiber mats, in which fiber diameters continuously increase with increasing DCD [134]. In this study, MB TPU fibers are found to be less entangled at shorter DCDs; however, the fibers collected on the rotating drum collector are oriented with increasing DCD instead of being randomly distributed as shown in **Figure 13**. The different fiber diameter formation and attenuation mechanisms during the melt blowing process may have been due to the differences in the thermal and elastic relaxations of TPU compared to commonly used polyolefins such as PP.

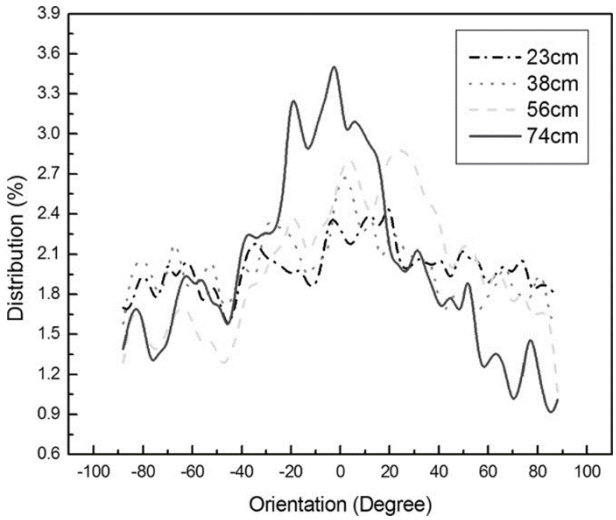

Figure 13. Distribution of the MB TPU fiber bundle orientation at various DCDs [134]

The fiber formation mechanism and the fiber structure developments highly dependent on the DCD beyond doubt. In general, lower DCDs yields thicker fiber diameter and lower porosity of the MB fibers. When DCD increases, fibers undergo higher attenuation, and therefore fiber diameter and porosity decrease while too large DCDs might cause severe imperfections. However, thermoplastic elastomers exhibit phenomenologically different fiber formation mechanism considering DCD conditions due to their thermal and elastic relaxation behavior (rubbery

characteristics). Consequently, the structure and properties of MB fiber mats can be controlled and optimized through DCD.

4. Developments of filter media made of MB nano/microfibers for filtration

The outbreak of the coronavirus (COVID-19) pandemic revealed that respiratory protection plays a vital role in the present world and the development of ultrafine polymeric fiber mats highly efficient filters allowing filtration of a wide range of particles, viruses, and aerosol is necessary [135, 136]. MB filters are the classic filtration media of good-quality masks, independent from the pandemic. Bioaerosols that are living or originate from living organisms might include microorganisms and fragments, toxins, and particulate waste from all varieties of living bodies [137]. These biologically hazardous substances or bioaerosols might be transferred through the air, and they could cause severe health effects because of their ability to incubate, grow, multiply, and produce toxic substances [138]. The efficient inhaled air filtration and cleaning off such hazardous particles, as well as the destruction of the inhibition of that bioaerosol development, are the matter of respiratory protection systems made of nonwovens filters. Many particulate respirators use a filter media made of MB fiber mats to capture these types of particles. We summarized the MB fiber mats and related properties in Table 3 reported for high-efficiency fiber mats produced via melt blowing technology.

Table 3. Some essential filtration properties of MB fiber mat filter medias reported in the literature

Material	Average fiber diameter [µm]	Average pore size [µm]	Porosity [%]	Pressure drop [Pa] (loading speed)	Filtration efficiency [%]	Reference
PP	0.55	6.5	N/A	54.9 (32 L/min)	81.9	[108]

PP	2.8	N/A	85.6	55.9 (0.053 m/s)	88.6	[139]
PP	2.4	9.3	N/A	37.4	95.91	[46]
2 layers PP MB + 3 layers PP Needle Punched (NP)	2.07 (MB) 17.9 (NP)	15.5 (MB) 70.1 (NP)	N/A	136.87 (85 L/min)	99.52	[140]
PP	0.47	N/A	N/A	20.27 (0.05 m/s)	91.19	[141]
0.5 wt% MgSt additive PP	1.63	~15	89.3	82.32 (85 L/min)	99.03	[142]
1 wt% MgSt additive PP	~2	14.2	90.1	53.1 (85 L/min)	92.57	[143]
PP MB + PVA ES	0.208	N/A	N/A	34 (3.4 m^3/h)	96.5	[144]
PP / PS	3	~9	~90	37.73 (32 L/ min)	99.87	[94]
Spunbond (PET/PE) / + TiO_2/Ag additive MB PP	4-16	3.3-3.8	N/A	~80 (85 L/ min)	~ 95	[52]
PP	2.64	~17	N/A	22.45 (0.053 m/s) @50 °C 19.45 (0.053 m/s) @110 °C	98.46 ~60	[145]
PP	2.1	11.2	89	120 (0.141 m/s)	99.65	[146]
PP / PEG	1-6	N/A	88	55.53 (0.053 m/s)	85.33	[147]
PP	1–2	3-14	89.94	38.7 (32 L/min)	98.35	[8]
10 %wt $BaTiO_3$ additive PP	~3	N/A	65	95 (0.053 m/s)	99.97	[148]
3 wt% TiO_2 additive PP	6.73	N/A	N/A	40 (85 L/ min)	96.32	[149]
PP / PC	0.63	N/A	N/A	59 (3.4 m^3/h)	95.9	[150]

PLA	0.1–3.0	N/A	N/A	40.8 (0.053 m/s)	88.5	[151]
PLA / PCL	3.3	N/A	N/A	N/A (0.053 m/s)	95	[152]
PLA	3.1	N/A	88.5	38.2 (0.053 m/s)	93.2	[139]

In order to fulfill various requirements considering an efficient filtration, multi-layer or laminated filtering systems are preferred, in which every layer meets different tasks. The MB fiber mats are often used as stacks that consists of several layers of the separate fiber mats and stacking of layers with another woven or nonwoven or a film [153, 154]. The additional layer for the filter is selected to impart additional or complementary properties to fulfill required features, such as tear resistance, strength, biocompatibility, air permeability and filtration properties. The laminated structures are highly suitable not only for respiratory devices but also for various application field including protective garments, drapes, medical gowns, covers for diapers, adult care products, sanitary napkins, etc. [155].

Roh *et. al.* [156] prepared and tested the filtration efficiency of multi-layered nonwoven filters made of electret PP MB fiber mat and PET nonwoven to lower the pressure drop, improve the quality and extend the service life for various filtration application. In their study, various filters were constructed with and without an air gap between the layers either by inserting a 5 mm thick acrylic plate (Air gap) or 5.5 mm thick-spacer web (S-gap) (**Figure 14**). The pressure drop across the filter media is a function of the particle loading speed; when loading speed increases, pressure drop increases. They reported that pressure drop decreases dramatically with NaCI particle loading when the air gap is inserted between layers. The designed air gap acted as the active flow channel between fiber mat stacks. However, the pressure drop with the loading did not effectively reduce

even increased for the tested the two layers construction spacer web inserted filter because of the thick spacer web inhibited airflow.

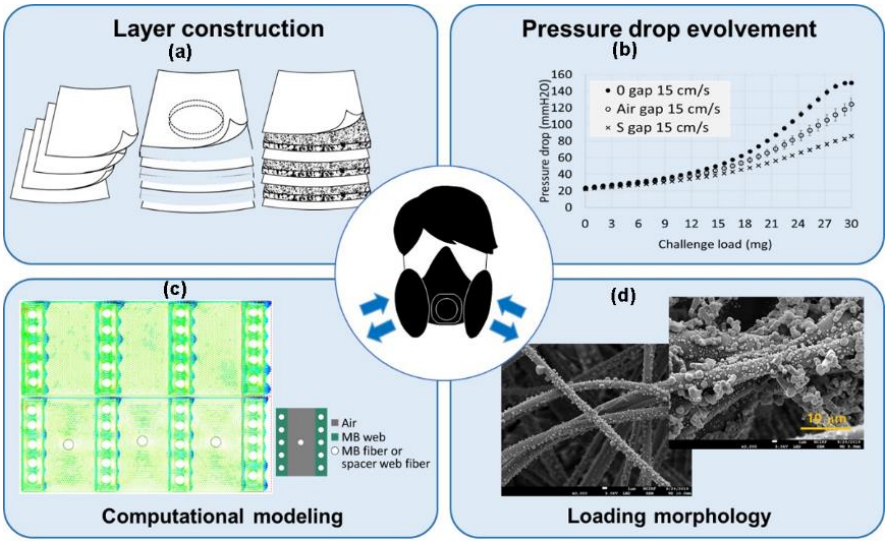

Figure 14. Schematic overview of the study (a) Filtering media layer construction, (b) Pressure drops of different layer-constructions for face velocity of 15 cm/s, (c) computational model for the pressure drop behavior of different stack and (d) Filter media morphology of different constructions after NaCI aerosol loading [156]

For the four-layer constructions, either the air gap or the spacer web insertion is found beneficial in reducing the pressure drop. Even, the effect was more significant when the loading velocity increased from 15 to 20 m/s. They obtained that spacer web insertion between the filter layers is more effective in reducing the pressure drop compared to using bulk air gap. Results obtained by the researchers showed that the inserted spacer web took place effectively distributing the airflow and pressure drop over the filter media because the thick spacer web acted as a direct airflow channel. A significant change in filtration efficiency and pressure drop occurs when the solid particles are accumulated inside a fiber mat medium. The pores of the fiber mats could be clogged with increasing pressure drop by the dendritic structure forming due to the captured solid particles. This is related to the pressure drop development, which goes faster for the solid aerosol particles

compared to the liquid aerosol of the filtering media [45]. They reported that layered filter design delays the clogging compared to the single layer MB fiber mats. However, increasing NaCI aerosol particle loading velocity from 15 cm/s to 20 cm/s increased the pressure drop and resulted in faster clogging of the filtering media. On the other hand, four-layered stacks showed promising results that successfully lowered the pressure drop and increased the service life of filter media by inserting either a spacer web or bulk air gap. Their results showed that the four-layered web spacer gap design has the most effective load share of solid particles via the uniform airflow distribution, besides no particle appeared in the bottom 4th layer (**Figure 15**). Furthermore, they determined that the four-layered web spacer gap design the loaded NaCI particles are shared from the 1st, 2nd, and 3rd MB layers with 87.7%, 9%, 3.3%, respectively.

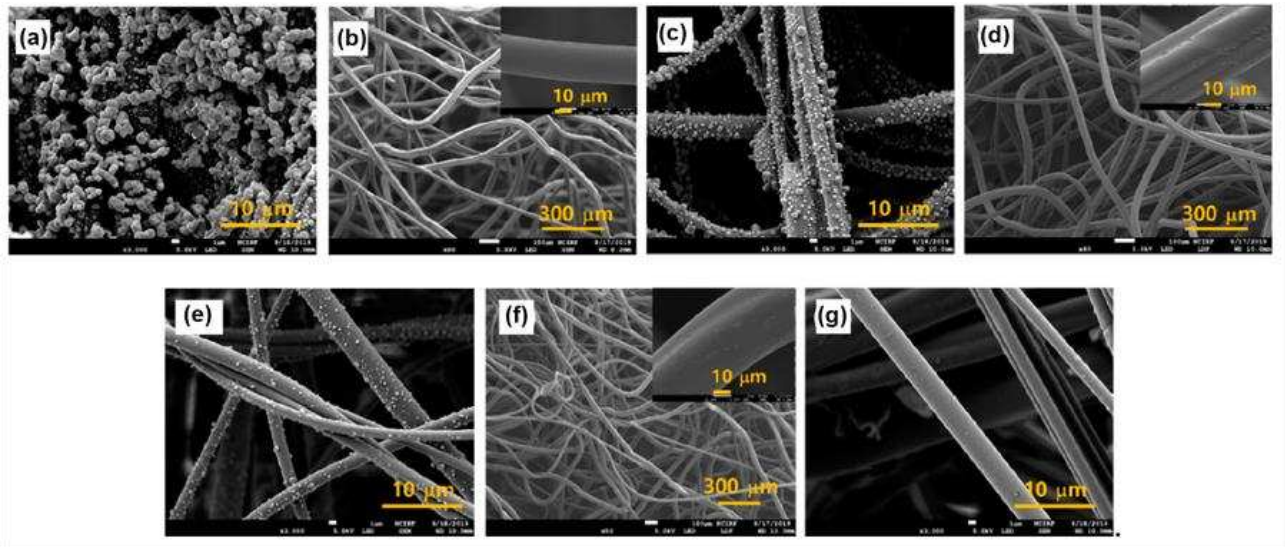

Figure 15. Four-layered stacks with spacer webs; (a) 1st MB layer (b) 1st spacer web layer, (c) 2nd MB layer, (d) 2nd spacer web layer, (e) 3rd MB layer, (f) 3rd spacer web layer, (g) 4th MB layer [156]

Li et. [144] developed a hierarchical fibrous structure made of PP MB and polyvinyl alcohol (PVA)/zeolite imidazole (ZIF) electrospun (ES) fibers. They produced PP MB and PVA/ZIF ES fiber mats separately, then they compressed the fiber mats to obtain composite fibrous structure.

The average fiber diameter of the hierarchical fibrous structure was around 0.209±0.058 μm in the most successive case. They observed that the hierarchical PM2.5 filtration performance improved to 96.5% while the pristine PP MB fiber mat had 21%. The hierarchical filter structure with finer fibers effectively intercepts the particles to acquire better adsorption, resulting in improved filtration efficiency. They also reported that composite filter media had higher tensile strength than that of the pristine fiber mats. This is associated with high friction and good fiber adhesion between the MB and ES fiber mats.

PP is the most widely used polymer for producing MB fiber mats [96] because of the fair mechanical properties and cheap price. It is a non-polar polymer having a very large band gap above 8 eV, which makes PP fiber mat a good electric insulator. This also makes PP less attractive for capturing tiny particles that is clearly a disadvantage. Admixing various charge enhancer additives (*e.g.,* barium titanate, stearate, calcium carbonate, etc.) are suggested to overcome this issue and hence improve the filtration performance [148, 157]. In addition, environmental conditions (*e.g.,* air humidity, moisture) and applied decontamination methods (*e.g.*, sanitizing with alcohol) may favor the degradation of the charge that reduces filtration performance [158]. Therefore, the ability to maintain charges is fundamental for various in-use scenarios such as in respiratory protective devices [27]. Electrostatic charging is frequently applied to nonwoven filters to enhance their tendency to capture smaller microorganisms. This is typical for particles smaller than a micron that can potentially penetrate into the respiratory system [159, 160]. These systems involving charged filter media are often called electret filters. Imparting electrostatic charge on the filter medium has been successfully applied in the last three decades to the fiber mats to improve filtration characteristics without compromising other properties (*e.g*., dimension and structure). Particularly, the ionic species generated by the negative polarity through the corona-charging is

proved to be an effective method to enhance filtration efficiency of MB PP fiber mats [160, 161]. Besides that, thermal preconditioning of the fiber mat may also enhance the static charge capacity by maintaining fiber mat interaction with the humid ambient air [8].

The performance of an electret filter efficiency is related to its electrostatic decay time. The filter media cannot capture small particles if the electrostatic capacity decays fast. Yang *et al.* [162] studied influence of corona discharge treatments on MB PP electret filters. They tested various levels (10-25 kV) of surface voltages with different discharging times (2-10 minutes) applied at room temperature (25 °C). They found that an increase in charging voltage and charging time reduces the surface resistance, resulting in higher air permeability for efficient filtration. They also reported that the MB fiber mat charged at 25 kV for 10 minutes maintains a high surface voltage for two weeks. Time is a limiting factor in civil use but can be feasible in industrial applications.

Brochocka [163] produced PP (MFI: 800 g/10 min @230 °C, 2.16 kg) MB electret filters by the addition of a superabsorbent polymer (SAP) with grain size of 250 μm and 30 μm. In the study, MB electret fiber mats were manufactured. They used an in situ electrostatic activation device cooperating melt blowing apparatus for the electrostatic charging of MB PP fibers. Besides the melt blowing apparatus used in this study enabled introducing SAP into molten PP. the effect of SAP grain sizes and electrostatic charge conditions (charged and non-charged) were tested according to the requirements for respiratory protective devices (EN 149:2001+A1:2009 and EN 13274- 7:2008). The filtration efficiency of the charged fiber mats was found significantly higher compared to the non-charged ones, but the grain size of SAP did not influence the filtration efficiency. The MB fiber mats containing SAP absorbed air moisture performed much better than those without SAP, which means a straightforward fiber making method can also contribute potential applications in personal protective devices (*e.g.* hygienic products with fast absorption

capability and storage of body fluids like urine, blood, etc.). The results show that partially embedded grains of the modifier in PP MB fibers did not compromise significant changes in the fiber structure (without hindering the functionality of the modifier). And electrostatic activation led to the physical modification of fibers that, in turn, gave higher filtration efficiency. She proved that MB fiber mat structures with high filtration efficiency designed for respiratory protective devices can be produced in one technological process.

In another study, Cheng *et. al.* [8] investigated the influence of electret temperature on the structure and filtration properties of PP MB fiber mats. In their study, a combined corona-temperature treatment method on the MB fibers was tested, that included a heat treatment (varied between 20-110 °C) while polarizing the filters. They found that increasing the electret temperature, the porosity decreases while the areal weight increases. They obtained through the wide-angle X-ray diffraction (WAXD) analysis that the increased electret temperature increased the diffraction peak signal of the 110, 040, 130 and 041 crystal planes of the PP α-crystals in the vicinity of 13.9°, 16.8°, 18.5°, and 22°. That translates the growth of the α crystal, and that resulted in higher degree of crystallinity of the fiber mats as shown in **Figure 16**. Increasing polymer crystallinity might be attributed to the nature of melt blowing, because the fast cooling of fibers might be affected crystallization kinetics. The rise of the α crystal's peak signal might be due to the complete crystallization of these domains at the temperature applied. Besides, they reported that the filtration efficiency depends on the crystallinity. They found that as the fiber crystallinity increases, filtration efficiency increases and vice versa, except at the highest electret temperature treatment (**Figure 17**). Increasing efficiency with increasing crystallinity is attributed to improved mechanical properties of the PP fiber mat. For the samples with low crystallinity, charging velocity might damage the fiber mat structure (*e.g.,* broadening the pore size). Higher crystallinity yields

higher tensile strength. Increasing crystallinity might improve mechanical properties in general, which gives a well-consolidated and robust filter media against the gas flow. The pressure drop test also showed an increasing trend with increased electret temperature and so fiber crystallinity. Therefore, the MB PP fiber mat's filtration efficiency improved with increasing electret temperature and fiber crystallinity against the NaCI charging with the applied constant velocity (5.33 cm/s). On the other hand, the decrease in filtration efficiency is associated with decreasing mat thickness for the highest electret temperature applied; however, no significant change observed for the rest of the samples.

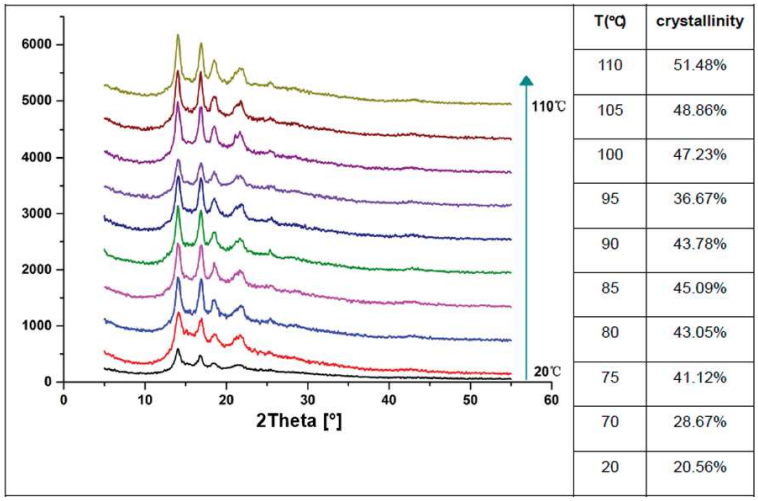

T(°C)	crystallinity
110	51.48%
105	48.86%
100	47.23%
95	36.67%
90	43.78%
85	45.09%
80	43.05%
75	41.12%
70	28.67%
20	20.56%

Figure 16. WAXD signals for various corona-temperature treated PP fiber mats [8]

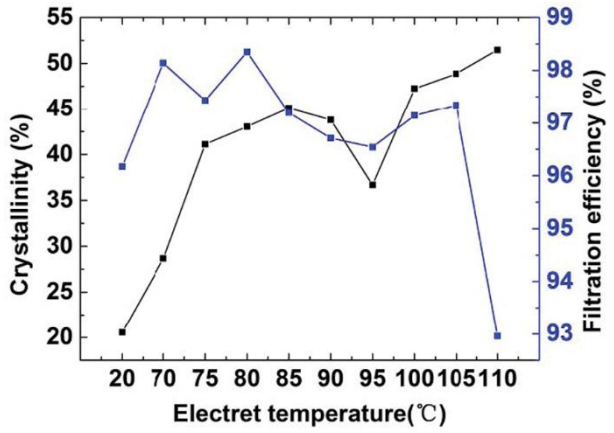

Figure 17. Change in the crystallinity and filtration efficiency respect to the electret temperature [8]

Kilic *et. al.* [148] compounded PP with various $BaTiO_3$ concentrations (0.1, 1 and 10 %wt) to enhance the performance of PP MB filters. In their study, $BaTiO_3$ particles were dispersed uniformly within the PP fibers without a compatibilizer. The average fiber diameter slightly decreased with increasing $BaTiO_3$ concentration (**Figure 18**). They heated the fiber mats at 130 °C and charged them at 9 kV for 10 minutes, and the filtration properties of the fiber mats were tested with dioctyl phthalate (DOP) aerosols in 20-300 nm range at a velocity of 5.3 m/s. They reported that thermal charging reduced DOP penetration from 14 to 7.3% in the case of 10% $BaTiO_3$ loaded PP MB fiber mats. They concluded that the applied method provides a filtration efficiency of 99.97% for the 300 nm particle size, which stands for KN100 grade respiratory protection devices. Besides that the efficiency of 10 min thermally charged 1% $BaTiO_3$/PP sample showed 90.8% filtration efficiency, whereas cold charged (without heat) exhibited 78.9% sample. These results show that more uniform and effective charging occurred for heated and charged fiber mats, resulting in higher filtration efficiency. On the other hand, their results showed that increasing the $BaTiO_3$ and thermal charging improved the polymer crystallinity and resulted in effective charge stability and hance enhanced filtration efficiency .

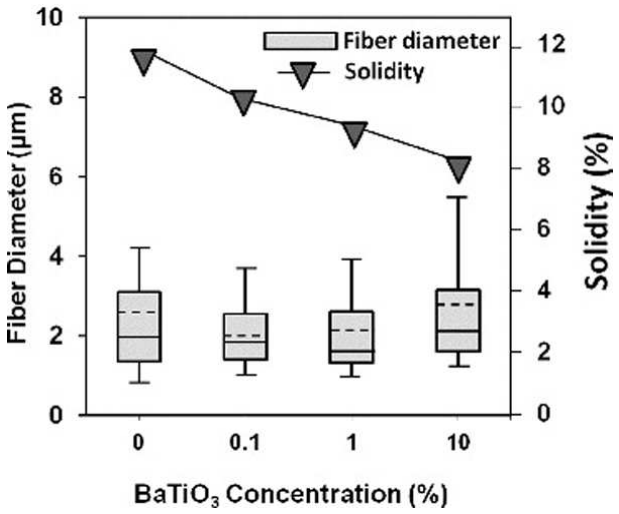

Figure 18. Change in MB fiber diameter and solidity versus $BaTiO_3$ concentration [148]

Zhang *et. al.* [143] reported that the addition of magnesium stearate (MgSt) to the PP melt improved MB fiber mats crystallinity, their electrostatic potential, as well as the filtration properties and the air permeability. They applied corona charging to further improve the filtration efficiency of the composite fiber mats. In their study, they made a systematic comparison of the filtration properties of the PP/MgSt fiber mat with a commercial MB fiber mat (PP, basis weight: 40 g/m^2, $d_{average}$:1.98 µm, thickness:0.41 mm, porosity:89%) and a commercial electrospun fiber mat (PAN, basis weight: 8.2 g/m^2, $d_{average}$:0.36 µm, thickness:0.05 mm, porosity:86%). The composite MB fiber mat (0.5 %wt MgSt additive PP) showed higher filtration efficiency against solid particles with a better thermal and humidity stability than the commercial electrospun and MB fiber mats (**Figure 19** (a)-(e)). On the other hand, increasing basis weight means more fibers in the filter media and that results in higher filtration efficiency; however, the developed composite fiber mat with 40 g/m^2 exhibited a filtration efficiency of 99% and a pressure drop less than 120 Pa, which stands for the FFP3 standard. The ratio of the negative natural log of penetration to the pressure drop gives the quality factor, which describes the dynamic filtration performance of air

filters. The quality factors of all samples decreased by increasing particle loading time. The commercial electrospun and MB fiber mats showed lower quality factors upon increasing particle loading time compared to the PP/MgSt fiber mats. On the other hand, the sharply declining trend of the electrospun fibers in quality factor with increasing loading lied behind the pore size. The authors concluded that the filter media having finer fibers with small pores led to forming a dendritic structure and clogs the pores by longer loading times (Figure 19 (f)), which in turn gives increasing pressure drop and therefore decrease the quality factor of the filter media. This results showed that the developed composite fiber mat was characterized by excellent electrostatic stability ensuring long storage and operating times.

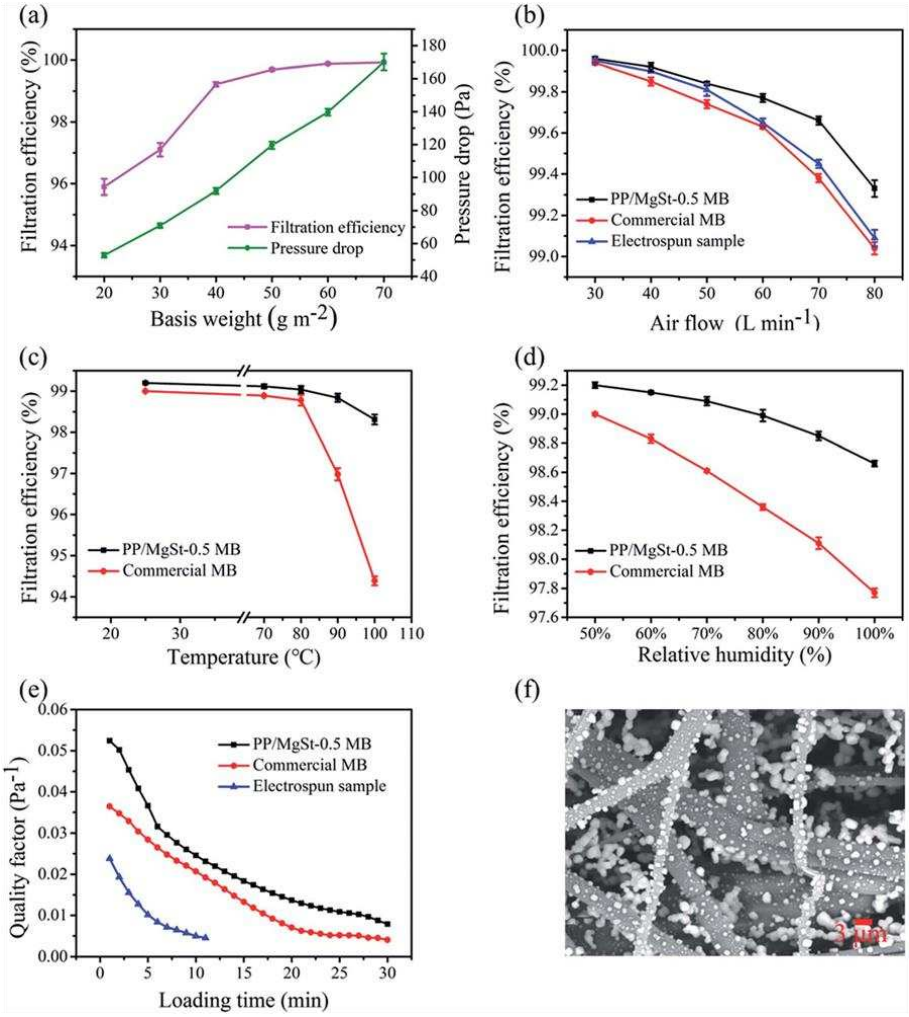

Figure 19. Filtration performance of the PP/MgSt MB fiber mat compared to the commercial electrospun and MB fiber mats (a) Filtration efficiency versus various basis weights (air flow rate of 85 L/min), (b) filtration efficiency versus various airflow rates, (c) the thermal stability of the filtration efficiency (air flow rate of 85 L/min), (d) humidity stability of the filtration efficiency (air flow rate of 85 L/min), (e) the quality factor respect to loading performance (air flow rate of 85 L/min), (f) the SEM images of the PP/MgSt samples after the loading filtration test [143]

A limited supply good quality respirator during the COVID-19 pandemic revealed that existing supply chains did not meet the surge in demand. This situation brought out a new route that paves

the way for the re-use of respiratory protection devices. In general, such respirators are made to be discarded after use. Re-using such respirators could significantly reduce the filtration performance, and that causes severe health issues for the user. A case study done by Hossain *et. al.* [164] presented an efficient way to maintain the filtration efficiency of used N95 respirators by re-charging the filter media after a decontamination procedure. They tested the filtration efficiency of several commercial masks supplied to hospitals made of PP MB fiber mats after sanitizing and re-charging them. They sanitized a N95 respirator by dipping it in ethanol and dried overnight. In the first step, they recharged the N95 respirator at 1 kV for 2,200 seconds and they obtained a filtration efficiency of about 86%. After that they sanitized the mask again by spreading 1 ml ethanol on the mask at the charging time of 3,125 seconds (measured filtration an efficiency of around 70%) and finally they removed the sample from the tester at 4,500 seconds and dried it by a hot air steam at 50 °C. They reported that the applied method decreased the filtration efficiency to 50% (**Figure 20** (a)) due to the pores blocked with residual alcohol. In these experiments they handled the sample extensively by attaching and detaching the tester. In the second method, the edges of the mask have been taped to prevent leakage from sides, and they applied *in-situ* recharging at 1,000V for 9,000 seconds after the same sanitizing process. Finally, they obtained 90% filtration efficiency by the *in-situ* recharging method (**Figure 20** (b)). Their results showed that the filtration efficiency of the respiratory devices made of PP MB fibers could somewhat recover by recharging the masks after sterilization; that method makes it possible to re-use N95 masks.

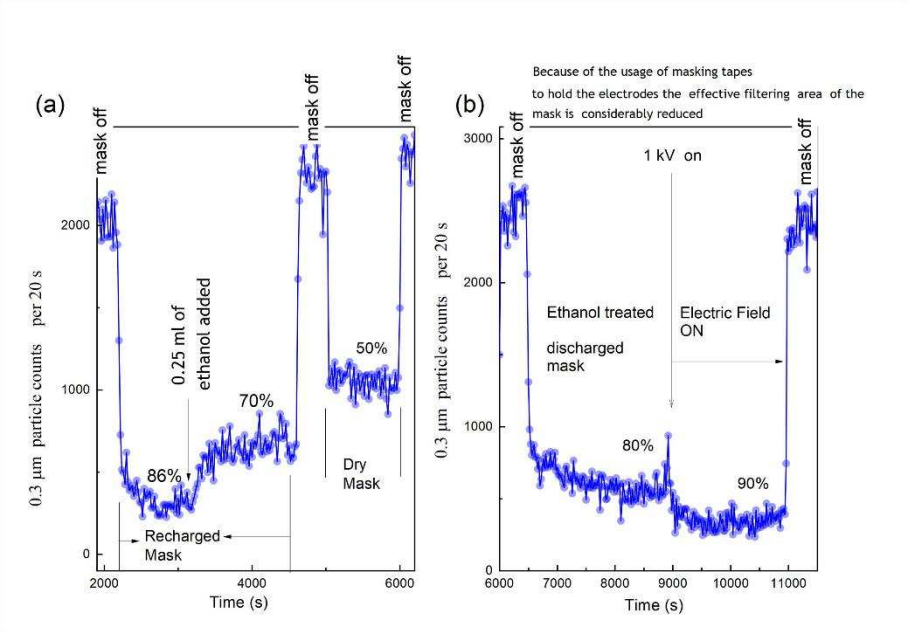

Figure 20. (a) Effect of 0.25 ml of ethanol on the filtering efficiency of the recharged commercial N95 mask (b) Effect of 1kV voltage applied across *in-situ* recharged commercial N95 mask [164]

Zhang *et. al.* [140] developed a PP multilayer composite filter made of needle-punched layer (NPL) and MB fiber mat layer (MBL) with a high filtration efficiency up to 99.52 ± 0.01% and a low-pressure drop of 136.87 ± 0.49 Pa as shown in **Figure 21**. They reported that hierarchical fibrous structure of 3 NPL / 2 MBL exhibited a dust holding capacity of 23.5 ± 0.41 g/m^2. High dust holding capacity translates a long service life for air filter. They observed that the multilayered filter's dust holding capacity (3NPL/2 MBL) with a basis weight of 190 g/cm^2 was also 3-fold higher than individual needle-punched and MB fiber mats having a basis weight of 200 g/cm^2 and 40 g/cm^2, respectively.

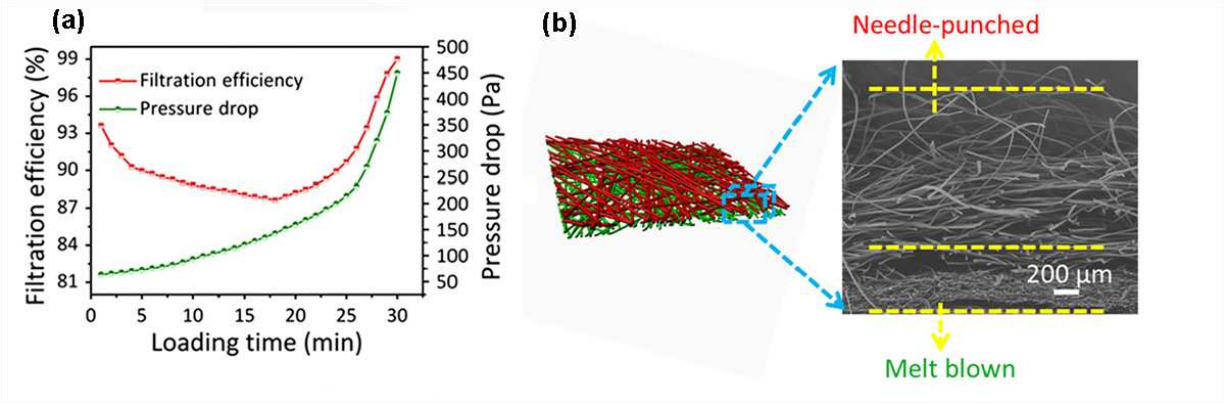

Figure 21. PP multilayer filter media (a) filtration efficiency and pressure drop under loading test and (b) structural construction [140]

MB fiber filters made of two or more polymer blends are developed to carry out to enhance the functionality at various filtration applications. Yu *et. al.* [152] prepared MB fiber mats made of PLA/PCL to create biocompatible filter media. They aimed to reduce the rigidity of the PLA with PCL compounding to achieve flexible MB fiber mats for filtration application. They found that blending PLA/PCL resulted in poor dispersion and uneven fiber morphology with increasing the PCL content due to the weak miscibility of the constituents. Therefore, they used tributyl citrate (TBC) 3 wt% to PCL weight as compatibilizer in PLA/PCL blends. It is found that the average fiber diameter of the PLA/PCL fiber mat increased from 5.2 µm to 7.9 µm with increasing PCL content from 1 to 5% while the degree of crystallinity rose from 25% to 30%. In their study, the flexible PLA/PCL fiber mat with an average diameter of 3.3 µm had a 95% filtration efficiency in the most successive case (**Figure 22**) that is equivalent to the KN95/FFP2 masks. They concluded that compounding PCL (up to 5 %wt) improved the crystallinity, tensile strength, ductility and air permeability of poly (lactic acid) MB fiber mats.

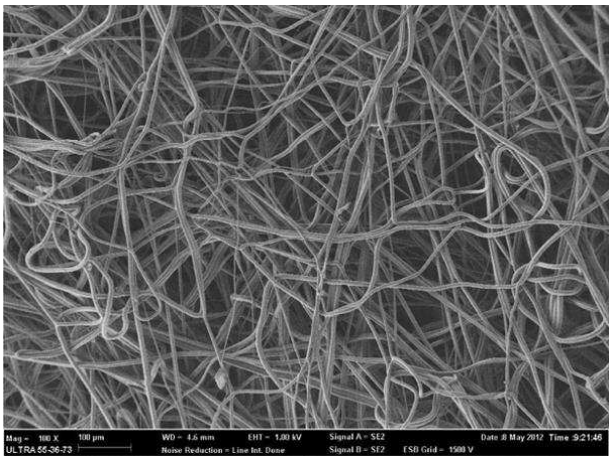

Figure 22. SEM image of a PLA/PCL MB fiber mat with average diameter of 3.3 μm [152]

Majchrzycka [165] developed a bioactived respiratory protection system made of PLA MB fiber mats to achieve high filtration efficiency against bioaerosols. In her study, a biocide-bioperlite (biocidal compounds harmless to human health) was prepared and applied to the fiber mats in order to activate fibers against bioaerosols. Additionally, a corona discharge (with a discharge of 30 kV) was applied to the fiber mats to improve the bioaerosol filtration efficiency. She reported that bioactivated electret PLA/bioperlite fiber mats achieved 99.34% and 99.26% filtration efficiency against Staphylococcus Aureusand and Pseudomonas Aeruginosa bacteria, respectively. However, the non-electrostatic activated PLA/bioperlite fiber mats exhibited 97.64% and 97.62% filtration efficiencies against the same bacteria, which makes these filters in the class of FFP2. They also obtained that the growth inhibition can be achieved for microorganisms (Staphylococcus Aureusand and Pseudomonas Aeruginosa) during the time of incubation at a temperature of 37 °C after 2 hours for the sample modified with bioperlite and electrostatically activated (**Figure 23**). Their results showed that bioaerosol incubation properties of the MB filter media made of the modified and electrostatically charged biocompatible polymers could be improved against without sacrificing filtration properties.

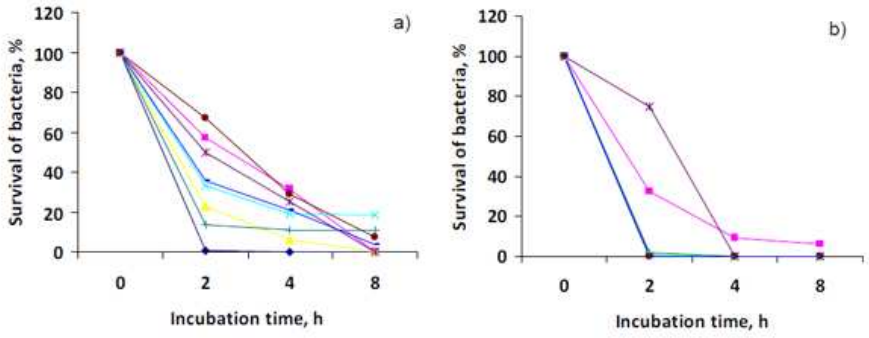

Figure 23. Results of tests on survival of (a) Staphylococcus aureus and (b) Pseudomonas Aeruginosa respect to time (colored lines represent various fiber mat sample tested) [165]

Zhu *et al.* [52] developed a high efficiency air filter by the incorporation of TiO_2/Ag nanoparticles into the composite nonwovens made of PET/PE spun-bonded (SB) - PP MB structure. They reported that the exposed TiO_2 nanoparticles on the fiber surface generated positive hole–negative electron pairs to produce OH radicals and superoxide radical anion under UV light as shown in Figure 24. The composite nonwoven filters achieved 99.07% and 99.27% antibacterial removal rate under UV light against E. coli and S. aureus, respectively. On the other hand, pristine SB / MB filter media without TiO_2/Ag nanoparticles had less than 20% antibacterial removal rate with and without UV treatment.

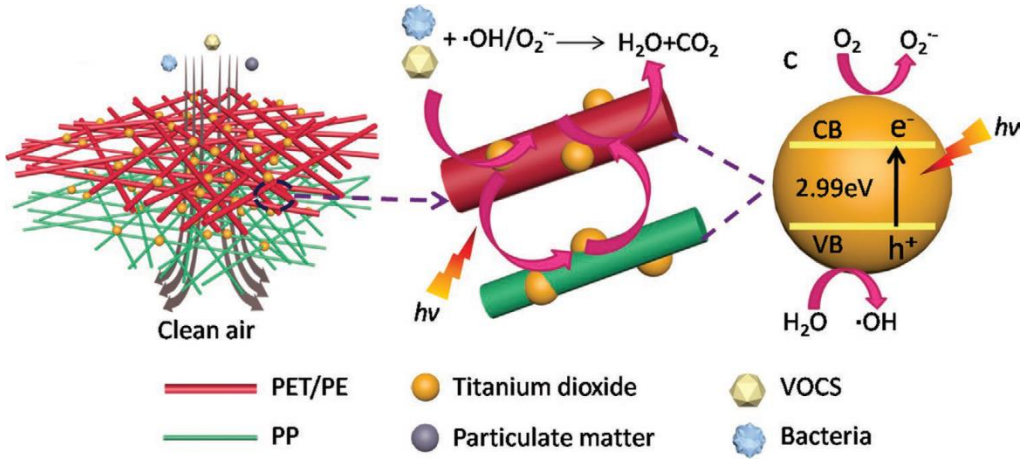

Figure 24. Mechanism schematic of simultaneous effect of composite nonwoven filter media for air pollutant removal and photocatalytic degradation of volatile organic compounds [52]

5. Conclusion

Melt blowing consists of the extrusion of a polymer through small orifices in a die with drawing of the extrudate by the aid of high-velocity hot air jets to generate continuous, fine polymeric fibers in the form of a nonwoven. Melt blowing is the one of the most efficient methods to produce fiber mats for filtering particulate matter, consisting of solid particles, liquid aerosol, and gas and vapor compounds beyond a doubt. To date, both industry and academy put considerable effort into the development of the MB fiber mats for the filtration applications. There are still many challenges for further optimization, end-product designing, characterization, and process modeling in practice despite the advances in the development of MB fiber mats for filtration implementation. Generally speaking, mostly polyolefins and commodity thermoplastics resins are the raw materials of MB products. Due to the fact that MB fibers process is often employed using polypropylene to manufacture commercial fiber mats, especially producing filter media for widespread application fields. The processing parameters is chosen to provide for filtration properties such as the fineness and evenness, pore size, strength, fiber diameter, thickness and air permeability, whereas the

materials are chosen to provide processability, strength, endurance and stability. The MB fiber morphology is very sensitive to processing parameters such as melt and polymer temperature, polymer throughput rate, air pressure, air temperature and die to collector distance (DCD). Fine fibers, therefore, high filtration efficiency fiber mat with small pore sizes can be produced by lowering the polymer throughput rate as long as all other parameters are the same. Increasing both air and polymer temperature, fibers tend to be attenuated more and usually finer fibers can be achieved by the reduced polymer viscosity. Besides, the crystallinity and orientation of the polymeric fiber can be developed by the increasing temperature; besides the mechanical and thermal properties of the fiber mat can be enhanced. Longer DCDs are favorable to decrease fiber diameter and increase porosity. Applying high air pressure is desired to attenuate further fiber diameter, which lowers the pore diameter and decreases the pressure drop. Nevertheless, the melt blowing parameters affecting do not going hand in hand but require a more in-depth process modelling for the application requirements accordingly. The MB fiber mats are often deployed as filters for high-performance respiratory applications, where the performance of breathing air filtration and boosting properties against bioaerosol capturing is highly demanded. The destructive impact of COVID-19 and work toward improving prevention against transmission of pandemic showed importance of the respiratory protection systems made of fibrous materials and so the fine fiber making methods. Developments are still ongoing, and it is still necessary to conduct further research improving the melt blowing and respiratory devices made of MB fiber mat. Precise control of solidity, porosity, pore size, fiber orientation, fiber entanglement, and forming thinner fibers (*e.g.,* < 500 nm) and utilizing specialty polymer structures (e.g., biopolymers) are still a challenge in industrial-scale filter media production. On the other hand, long-term maintaining and stabilizing electrical charges, reuse, recyclability, recycling of the filters, longer service life, filter

design, filtration performance in chemically and thermally challenging environments are remained to be solved in the future.

Acknowledgment

This paper created at the Budapest University of Technology and Economics was supported by the "TKP2020, Institutional Excellence Program" of the National Research Development and Innovation Office in the field of Nanotechnology and Materials Science (BME IE-NAT TKP2020). This paper was also supported by the János Bolyai Research Scholarship of the Hungarian Academy of Sciences (MTA), the by the ÚNKP-20-5 New National Excellence Program of the Ministry for Innovation and Technology and the Stipendium Hungaricum Scholarship of Tempus Public Foundation.

REFERENCES

1. Hassan MA, Yeom BY, Wilkie A, et al. Fabrication of nanofiber meltblown membranes and their filtration properties. *Journal of Membrane Science* 2013; 427: 336-344.

2. Leonas KK and Huang W. Transmission of small particles through selected surgical gown fabrics. *International Nonwovens Journal* 1999: 1558925099OS-1558800116.

3. Albrecht W, Fuchs H and Kittelmann W. Nonwoven Fabrics : Raw Materials, Manufacture, Applications, Characteristics, Testing Processes. 2002.

4. Bhat G and Malkan S. Polymer-laid web formation. In: Russell SJ (ed) *Handbook of nonwovens*. Cambridge (UK), 2007, pp.180-182.

5. Yesil Y and Bhat GS. Porosity and barrier properties of polyethylene meltblown nonwovens. *The Journal of the Textile Institute* 2017; 108: 1035-1040.

6. Brochocka A and Majchrzycka K. Technology for the production of bioactive melt-blown filtration materials applied to respiratory protective devices. *Fibres & Textiles in Eastern Europe* 2009; 17: 92-98.

7. Majchrzycka K, Brochocka A and Grzybowski P. Modelling the viability of microorganisms of poly (lactic Acid) melt-blown nonwoven fabrics for the use of respiratory protection. *Fibres & Textiles in Eastern Europe* 2015.

8. Cheng S, Muhaiminul AS, Yue Z, et al. Effect of Temperature on the Structure and Filtration Performance of Polypropylene Melt-Blown Nonwovens. *Autex Research Journal* 2020; 1.

9. Angadjivand SA, Brandner JM and Springett JE. *Molded respirator comprising meltblown fiber web with staple fibers*. USA, 2011.

10. Pinchuk L, Goldade V, Makarevich A, et al. Introduction (Historical Review). In: Pinchuk L, Goldade V, Makarevich A, et al. (eds) *Melt Blowing Equipment, Technology, and Polymer Fibrous Materials*. Berlin: Springer-Verlag Berlin Heidelberg, 2002, pp.1-3.

11. Erben J, Pilarova K, Sanetrnik F, et al. The combination of meltblown and electrospinning for bone tissue engineering. *Materials Letters* 2015; 143: 172-176.

12. Vadas D, Kmetykó D, Marosi G, et al. Application of Melt-Blown Poly (lactic acid) Fibres in Self-Reinforced Composites. *Polymers* 2018; 10: 766.

13. Wang H, Zhang Y, Gao H, et al. Composite melt-blown nonwoven fabrics with large pore size as Li-ion battery separator. *International Journal of Hydrogen Energy* 2016; 41: 324-330.

14. Balogh A, Farkas B, Farago K, et al. Melt-blown and electrospun drug-loaded polymer fiber mats for dissolution enhancement: a comparative study. *J Pharm Sci* 2015; 104: 1767-1776. 2015/03/13. DOI: 10.1002/jps.24399.

15. Souzandeh H, Wang Y, Netravali AN, et al. Towards Sustainable and Multifunctional Air-Filters: A Review on Biopolymer-Based Filtration Materials. *Polymer Reviews* 2019; 59: 651-686. DOI: 10.1080/15583724.2019.1599391.

16. Watanabe K, Kim B-S and Kim I-S. Development of Polypropylene Nanofiber Production System. *Polymer Reviews* 2011; 51: 288-308. DOI: 10.1080/15583724.2011.594195.

17. Gereffi G. What does the COVID-19 pandemic teach us about global value chains? The case of medical supplies. *Journal of International Business Policy* 2020; 3: 287-301.

18. Bai Y, Yao L, Wei T, et al. Presumed asymptomatic carrier transmission of COVID-19. *Jama* 2020; 323: 1406-1407.

19. Yesil Y and Bhat GS. Structure and mechanical properties of polyethylene melt blown nonwovens. *International Journal of Clothing Science and Technology* 2016; 28: 780-793. DOI: 10.1108/ijcst-09-2015-0099.

20. Koprivova B, Lisnenko M, Solarska-Sciuk K, et al. Large-scale electrospinning of poly (vinylalcohol) nanofibers incorporated with platelet-derived growth factors. *Express Polymer Letters* 2020; 14.

21. Guo C, Wang Q, Liu J, et al. Electrospun polyimide ultrafine non-woven fabrics with high whiteness and good thermal stability from organo-soluble semi-alicyclic polyimides: Preparation and properties. *Express Polymer Letters* 2019; 13.

22. Kara Y, He H and Molnár K. Shear-aided high-throughput electrospinning: A needleless method with enhanced jet formation. *Journal of Applied Polymer Science* 2020; 137: 49104. DOI: 10.1002/app.49104.

23. Zhang Z, Ji D, He H, et al. Electrospun ultrafine fibers for advanced face masks. *Materials Science and Engineering: R: Reports* 2021; 143: 100594. DOI: https://doi.org/10.1016/j.mser.2020.100594.

24. Pinchuk LS, Goldade VA, Makarevich AV, et al. Structure of Melt-Blown Polymer Fibrous Materials (PFM). In: Pinchuk LS, Goldade VA, Makarevich AV, et al. (eds) *Melt Blowing: Equipment, Technology, and Polymer Fibrous Materials*. Berlin, Heidelberg: Springer Berlin Heidelberg, 2002, pp.53-64.

25. Kara Y and Molnár K. Revealing of process–structure–property relationships of fine polypropylene fiber mats generated via melt blowing. *Polymers for Advanced Technologies* 2021: 1-17. DOI: https://doi.org/10.1002/pat.5270.

26. Liu J, Pui DY and Wang J. Removal of airborne nanoparticles by membrane coated filters. *Science of the total environment* 2011; 409: 4868-4874.

27. Hutten IM. Properties of Nonwoven Filter Media. In: Hutten IM (ed) *Handbook of Nonwoven Filter Media*. Oxford: Butterworth-Heinemann, 2007, pp.71-102.

28. GB 2626-2019. Respiratory protection—Non-powered air-purifying particle respirator.

29. R M and J S. NIOSH Fact Sheet, https://www.cdc.gov/niosh/docs/2011-179/pdfs/2011-179.pdf (2011, accessed 11 June 2020 2020).

30. Racz L, Yamamoto DP and Eninger RM. *Handbook of respiratory protection: Safeguarding against current and emerging hazards*. CRC Press, 2017.

31. Services USDoHH. Respirator Fact Sheet, https://www.cdc.gov/niosh/npptl/topics/respirators/factsheets/respsars.html (2020, accessed 11 May 2020 2020).

32. Li J, Gao F, Liu L, et al. Needleless electro-spun nanofibers used for filtration of small particles. *Express Polymer Letters* 2013; 7.

33. EN 149:2001+A1:2009. Respiratory protective devices - Filtering half masks to protect against particles - Requirements, testing, marking.

34. Respiratory protective devices. Methods of test. Determination of particle filter penetration.

35. Community face coverings - Guide to minimum requirements, methods of testing and use.

36. Shereen MA, Khan S, Kazmi A, et al. COVID-19 infection: origin, transmission, and characteristics of human coronaviruses. *Journal of Advanced Research* 2020.

37. Bałazy A, Toivola M, Adhikari A, et al. Do N95 respirators provide 95% protection level against airborne viruses, and how adequate are surgical masks? *American journal of infection control* 2006; 34: 51-57.

38. Tsai P and Yan Y. The influence of fiber and fabric properties on nonwoven performance. *Applications of nonwovens in technical textiles*. Elsevier, 2010, pp.18-45.

39. Yesil Y and Bhat GS. Porosity and barrier properties of polyethylene meltblown nonwovens. *The Journal of The Textile Institute* 2016; 108: 1035-1040. DOI: 10.1080/00405000.2016.1218109.

40. He H, Gao M, Illés B, et al. 3D Printed and Electrospun, Transparent, Hierarchical Polylactic Acid Mask Nanoporous Filter. *International Journal of Bioprinting* 2020; 6. Coronavirus disease-19, Electrospinning, Mask nanoporous filter, Nanofibers, Three-dimensional printing 2020-06-30. DOI: 10.18063/ijb.v6i4.278.

41. Motyl E and Lowkis B. Effect of air humidity on charge decay and lifetime of PP electret nonwovens. *Fibres and Textiles in Eastern Europe* 2006; 14: 59.

42. Mao N. Nonwoven fabric filters. In: Kellie G (ed) *Advances in Technical Nonwovens*. United Kingdom: Woodhead Publishing, 2016, pp.273-310.

43. Abd El-Hamied AE-HA. Investigation of Loaded Fibrous Filter. *Periodica Polytechnica Mechanical Engineering* 1997; 41: 3-20. DOI: N/A.

44. Tsai PP-y. Theoretical and experimental investigation on the relationship between the Nonwoven structure and the web properties. *International Nonwovens Journal* 2002: 1558925002OS-1501100408.

45. Thomas D, Contal P, Renaudin V, et al. Modelling pressure drop in HEPA filters during dynamic filtration. *Journal of aerosol science* 1999; 30: 235-246.

46. Xiao Y, Sakib N, Yue Z, et al. Study on the Relationship Between Structure Parameters and Filtration Performance of Polypropylene Meltblown Nonwovens. *Autex Research Journal* 2019; 1.

47. Wang Q, Maze B, Tafreshi HV, et al. A case study of simulating submicron aerosol filtration via lightweight spun-bonded filter media. *Chemical Engineering Science* 2006; 61: 4871-4883. DOI: https://doi.org/10.1016/j.ces.2006.03.039.

48. Jaganathan S, Vahedi Tafreshi H and Pourdeyhimi B. On the pressure drop prediction of filter media composed of fibers with bimodal diameter distributions. *Powder Technology* 2008; 181: 89-95. DOI: https://doi.org/10.1016/j.powtec.2007.07.002.

49. Ghosh S. Composite nonwovens in medical applications. In: Das D and Pourdeyhimi B (eds) *Composite Non-Woven Materials*. UK: Woodhead Publishing, 2014, pp.211-224.

50. Mukhopadhyay A. Composite nonwovens in filters: applications. In: Das D and Pourdeyhimi B (eds) *Composite Non-Woven Materials*. UK: Woodhead Publishing, 2014, pp.164-210.

51. Das D, Pradhan AK, Chattopadhyay R, et al. Composite Nonwovens. *Textile Progress* 2012; 44: 1-84. DOI: 10.1080/00405167.2012.670014.

52. Zhu X, Dai Z, Xu K, et al. Fabrication of Multifunctional Filters via Online Incorporating Nano-TiO2 into Spun-Bonded/Melt-Blown Nonwovens for Air Filtration and Toluene Degradation. *Macromolecular Materials and Engineering* 2019; 304: 1900350. DOI: https://doi.org/10.1002/mame.201900350.

53. Kothari VK and Newton A. The air-permeability of non-woven fabrics. *Journal of the Textile Institute* 1974; 65: 525-531.

54. Gombos Z. *Analysis of glass fiber mat structures and their impact on the resin absorption process and on the characteristics of composites*. Budapest University of Technology and Economics, Budapest, 2010.

55. Góra A, Sahay R, Thavasi V, et al. Melt-Electrospun Fibers for Advances in Biomedical Engineering, Clean Energy, Filtration, and Separation. *Polymer Reviews* 2011; 51: 265-287. DOI: 10.1080/15583724.2011.594196.

56. Wente VA. Superfine Thermoplastic Fibers. *Industrial & Engineering Chemistry* 1956; 48: 1342-1346. DOI: 10.1021/ie50560a034.

57. Player J. *Improvement in mineral wool*. Patent USRE6895E, USA, 1876.

58. Hall CC. *Process of making mineral-wool felt*. USA, 1903.

59. Thomas JH. *Apparatus for manufacturing glass wool*. USA, 1940.

60. Bryner M. *Extremely high liquid barrier fabrics*. USA, 2004.

61. Prentice JS. *Laminated non-woven sheet*. USA, 1978.

62. Grier-Idris C. *Conformable surgical face mask*. USA, 1987.

63. Coates DA and Smith RJM. *Disposable surgical face mask and method of producing it*. United Kingdom, 1981.

64. Bodaghi H, Erickson SC, Purrington SM, et al. *Oriented melt-blown fibers, processes for making such fibers and webs made from such fibers*. USA, 1999.

65. Van Paridon H, Tynys A, Fiebig J, et al. *Terpolymer for melt blown media for air filtration*. USA, 2016.

66. Haubruge H, Pavy G and Standaert A. *Fibres and nonwoven prepared from polypropylene having a large dispersity index*. USA, 2012.

67. Demain A. *Polypropylene fibres*. USA, 2003.

68. Barboza SD, Hoffman Jr CS, Kopp CV, et al. *Melt-blown filtration media having integrally co-located support and filtration fibers*. USA, 1997.

69. Wilson A. The formation of dry, wet, spunlaid and other types of nonwovens. In: Chapman RA (ed) *Applications of Nonwovens in Technical Textiles*. United Kingdom: Woodhead Publishing, 2010, pp.3-17.

70. Shambaugh R. L. A Macroscopic View of the Melt-Blowing Process for Producing Microfibers. *Industrial & engineering chemistry research* 1988; 27: 2363-2372.

71. Gahan R. and Zguris G.C. A review of the melt blown process. In: *In Battery Conference on Applications and Advances, The Fifteenth Annual IEEE* New Orleans (USA), 2000, pp.145-149.

72. Reicofil R. https://www.reicofil.com/en/pages/meltblown_lines (accessed 18 July 2020 2020).

73. Buntin RR. *Battery separators made from polymeric fibers*. Patent US3972759A, USA, 1976.

74. Ellison CJ, Phatak A, Giles DW, et al. Melt blown nanofibers: Fiber diameter distributions and onset of fiber breakup. *Polymer* 2007; 48: 3306-3316. DOI: 10.1016/j.polymer.2007.04.005.

75. Yu Y, Xiong S, Huang H, et al. Fabrication and application of poly (phenylene sulfide) ultrafine fiber. *Reactive and Functional Polymers* 2020; 150: 104539. DOI: https://doi.org/10.1016/j.reactfunctpolym.2020.104539.

76. Zhao R and Wadsworth LC. Attenuating PP/PET bicomponent melt blown microfibers. *Polymer Engineering & Science* 2003; 43: 463-469.

77. Zhang D, Sun C, Beard J, et al. Development and characterization of poly(trimethylene terephthalate)-based bicomponent meltblown nonwovens. *Journal of Applied Polymer Science* 2002; 83: 1280-1287. DOI: 10.1002/app.2295.

78. Brochocka A. Efficiency of electret polycarbonate nonwovens in respiratory protection against nanoparticles. *Autex Research Journal* 2017; 17: 188-198.

79. Safranski DL, Boothby JM, Kelly CN, et al. Thermo-mechanical behavior and structure of melt blown shape-memory polyurethane nonwovens. *J Mech Behav Biomed Mater* 2016; 62: 545-555. 2016/06/17. DOI: 10.1016/j.jmbbm.2016.05.038.

80. Wadsworth LC and Khan AY. *Meltblowing of ethylene and fluorinated ethylene copolymers*. United States 1995.

81. Ruamsuk R, Takarada W and Kikutani T. Fine filament formation behavior of polymethylpentene and polypropylene near spinneret in melt blowing process. *International Polymer Processing* 2016; 31: 217-223.

82. Hammonds RL, Gazzola WH and Benson RS. Physical and thermal characterization of polylactic acid meltblown nonwovens. *Journal of Applied Polymer Science* 2014; 131.

83. Yu Y and Shim E. Process-structure-property relationship of meltblown poly (styrene–ethylene/butylene–styrene) nonwovens. *Journal of Applied Polymer Science* 2021; 138: 50230.

84. Henry JJ, Goldbach J, Stabler S, et al. Advancements in the production of meltblown fibres. *Filtration + Separation* 2016; 53: 36-40. DOI: https://doi.org/10.1016/S0015-1882(16)30123-9.

85. Zhang D, Sun C, Beard J, et al. Innovative polytrimethylene terephthalate (PTT) polymers for technical nonwovens. *Journal of industrial textiles* 2002; 31: 159-178.

86. Müller DH and Krobjilowski A. Meltblown fabrics from biodegradable polymers. *International Nonwovens Journal* 2001: 1558925001os-1551000106.

87. Chen T, Wang X and Huang X. Effects of Processing Parameters on the Fiber Diameter of Melt Blown Nonwoven Fabrics. *Textile Research Journal* 2016; 75: 76-80. DOI: 10.1177/004051750507500114.

88. Yarin A. L., Pourdeyhimi B. and Ramakrishna S. Melt- and solution blowing. In: Yarin A. L., Pourdeyhimi B. and Ramakrishna S. (eds) *Fundamentals and applications of micro and nanofibers*. UK: Cambridge University Press 2013

pp.90-92

89. Ghijsels A and De Clippeleir J. Melt Strength Behaviour of Polypropylenes. *International Polymer Processing* 1994; 9: 252-257. DOI: 10.3139/217.940252.

90. Tan DH, Zhou C, Ellison CJ, et al. Meltblown fibers: Influence of viscosity and elasticity on diameter distribution. *Journal of Non-Newtonian Fluid Mechanics* 2010; 165: 892-900. DOI: 10.1016/j.jnnfm.2010.04.012.

91. Drabek J and Zatloukal M. Influence of long chain branching on fiber diameter distribution for polypropylene nonwovens produced by melt blown process. *Journal of Rheology* 2019; 63: 519-532.

92. Drabek J and Zatloukal M. Influence of molecular weight, temperature, and extensional rheology on melt blowing process stability for linear isotactic polypropylene. *Physics of Fluids* 2020; 32: 083110.

93. Jones A. M. A Study of Resin Melt Flow Rate And Polydispersity Effects On The Mechanical Properties of Melt Blown Polypropylene Webs. In: *Fourth International Conference on Polypropylene Fibers and Textiles* Nottingham (UK), September 23–25 1987

94. Deng N, He H, Yan J, et al. One-step melt-blowing of multi-scale micro/nano fabric membrane for advanced air-filtration. *Polymer* 2019; 165: 174-179. DOI: 10.1016/j.polymer.2019.01.035.

95. Xu QY and Wang YM. The Effects of Processing Parameter on Melt-Blown Filtration Materials. *Advanced Materials Research* 2013; 650: 78-84. DOI: 10.4028/www.scientific.net/AMR.650.78.

96. Dutton K.C. Overview and Analysis of the Meltblown Process and Parameters. *Journal of Textile and Apparel, Technology and Management* 2008; 6.

97. Zhang D, Sun C, Beard J, et al. Development and characterization of poly (trimethylene terephthalate)-based bicomponent meltblown nonwovens. *Journal of Applied Polymer Science* 2002; 83: 1280-1287.

98. Wang X and Ke Q. Experimental investigation of adhesive meltblown web production using accessory air. *Polymer Engineering & Science* 2006; 46: 1-7.

99. Velu YK, Ghosh TK and Seyam AM. Meltblown Structures Formed by a Robotic and Meltblowing Integrated System: Impact of Process Parameters on Pore Size. *Textile Research Journal* 2003; 73: 971-979. DOI: 10.1177/004051750307301107.

100. Guo M, Liang H, Luo Z, et al. Study on melt-blown processing, web structure of polypropylene nonwovens and its BTX adsorption. *Fibers and Polymers* 2016; 17: 257-265.

101. Marla VT and Shambaugh RL. Modeling of the Melt Blowing Performance of Slot Dies. *Industrial & Engineering Chemistry Research* 2004; 43: 2789-2797. DOI: 10.1021/ie030767a.

102. Bansal V and Shambaugh RL. On-line Determination of Diameter and Temperature during Melt Blowing of Polypropylene. *Industrial & engineering chemistry research* 1998; 37: 1799.

103. Bresee RR and Qureshi UA. Fiber Motion near the Collector during Melt Blowing: Part 2 — Fly Formation. *International Nonwovens Journal* 2002; os-11: 1558925002OS-1501100306. DOI: 10.1177/1558925002os-01100306.

104. Drabek J and Zatloukal M. Meltblown technology for production of polymeric microfibers/nanofibers: A review. *Physics of Fluids* 2019; 31: 091301.

105. Yeşil Y. Effect of Air Quenching on Characteristics of Thermoplastic Polyurethane Meltblown Nonwoven. *Journal of Textile & Apparel/Tekstil ve Konfeksiyon* 2015; 25.

106. Milligan MW and Haynes BD. Empirical models for melt blowing. *Journal of Applied Polymer Science* 1995; 58: 159-163. DOI: 10.1002/app.1995.070580117.

107. Xie S, Han W, Jiang G, et al. Turbulent air flow field in slot-die melt blowing for manufacturing microfibrous nonwoven materials. *Journal of Materials Science* 2018; 53: 6991-7003. DOI: 10.1007/s10853-018-2008-y.

108. Uppal R, Bhat G, Eash C, et al. Meltblown nanofiber media for enhanced quality factor. *Fibers and Polymers* 2013; 14: 660-668. DOI: 10.1007/s12221-013-0660-z.

109. Milligan MW, Lu F, Buntin RR, et al. The use of crossflow to improve nonwoven melt-blown fibers. *APP Journal of Applied Polymer Science* 1992; 44: 279-288.

110. Majumdar B and Shambaugh RL. Air drag on filaments in the melt blowing process. *Journal of Rheology* 1990; 34: 591-601.

111. Hao X and Zeng Y. A review on the studies of air flow field and fiber formation process during melt blowing. *Industrial & Engineering Chemistry Research* 2019; 58: 11624-11637.

112. Choi KJ, Spruiell JE, Fellers JF, et al. Strength properties of melt blown nonwoven webs. *Polymer Engineering & Science* 1988; 28: 81-89.

113. Bresee RR, Qureshi A and Pelham MC. Influence of processing conditions on melt blown web structure: part 2-primary airflow rate. *International Nonwovens Journal* 2005: 1558925005os-1551400202.

114. Tyagi MK and Shambaugh RL. Use of Oscillating Gas Jets in Fiber Processing. *Industrial & Engineering Chemistry Research* 1995; 34: 656-660. DOI: 10.1021/ie00041a027.

115. Tan DH, Herman PK, Janakiraman A, et al. Influence of Laval nozzles on the air flow field in melt blowing apparatus. *Chemical Engineering Science* 2012; 80: 342-348. DOI: 10.1016/j.ces.2012.06.020.

116. Xie S and Zeng Y. Fiber spiral motion in a swirl die melt-blowing process. *Fibers and Polymers* 2014; 15: 553-559. DOI: 10.1007/s12221-014-0553-9.

117. Jirsák O. and Wadsworth L.C. *Nonwoven Textiles*. USA: Carolina Academic Press, 1999.

118. Shambaugh BR, Papavassiliou DV and Shambaugh RL. Modifying air fields to improve melt blowing. *Industrial & engineering chemistry research* 2012; 51: 3472-3482.

119. Bo Z. Production of polypropylene melt blown nonwoven fabrics: Part I-numerical simulation and prediction of fibre diameter. *Indian Journal of Fibre and Textile Research* 2012; 37: 280-286.

120. Drabek J, Zatloukal M and Martyn M. Effect of molecular weight on secondary Newtonian plateau at high shear rates for linear isotactic melt blown polypropylenes. *Journal of Non-Newtonian Fluid Mechanics* 2018; 251: 107-118. DOI: https://doi.org/10.1016/j.jnnfm.2017.11.009.

121. Lee Y and Wadsworth LC. Effects of melt-blowing process conditions on morphological and mechanical properties of polypropylene webs. *Polymer* 1992; 33: 1200-1209.

122. Xie S, Zheng Y and Zeng Y. Influence of Die Geometry on Fiber Motion and Fiber Attenuation in the Melt-Blowing Process. *Industrial & Engineering Chemistry Research* 2014; 53: 12866-12871. DOI: 10.1021/ie5025529.

123. Moore EM, Papavassiliou DV and Shambaugh RL. Air Velocity, Air Temperature, Fiber Vibration and Fiber Diameter Measurements on a Practical Melt Blowing Die. *International Nonwovens Journal International Nonwovens Journal* 2004; 13: 1558925004os-1558925013.

124. Yin H, Yan Z, Ko W-C, et al. Fundamental Description of the Melt Blowing Process. *International Nonwovens Journal International Nonwovens Journal* 2000; 9: 1558925000OS-1558925090.

125. Begenir A, Michielsen S and Pourdeyhimi B. Melt-blowing thermoplastic polyurethane and polyether-block-amide elastomers: Effect of processing conditions and crystallization on web properties. *Polymer Engineering & Science* 2009; 49: 1340-1349.

126. Feng J. Preparation and properties of poly (lactic acid) fiber melt blown non-woven disordered mats. *Materials Letters* 2017; 189: 180-183.

127. Bresee RR. Fiber Motion Near The Collector During Melt Blowing Part 1: General Considerations. *International Nonwovens Journal* 2002: 1558925002OS-1501100207.

128. Das D. Introduction to composite nonwovens. In: Das D and Pourdeyhimi B (eds) *Composite Non-Woven Materials*. United Kingdom: Woodhead Publishing, 2014, pp.1-19.

129. Chen T, Li L and Huang X. Fiber diameter of polybutylene terephthalate melt-blown nonwovens. *Journal of Applied Polymer Science* 2005; 97: 1750-1752. DOI: 10.1002/app.21932.

130. Bresee RR and Qureshi UA. Influence of process Conditions on Melt Blown Web Structure. Part IV - Fiber Diameter. *Journal of Engineered Fibers and Fabrics* 2006; 1: 155892500600100.

131. Bo Z. Production of polypropylene melt blown nonwoven fabrics: Part II-Effect of process parameters. *INDIAN JOURNAL OF FIBRE AND TEXTILE RESEARCH* 2012; 37: 326-330.

132. Qureshi UA. *Understanding the role of the collector during melt blowing*. University of Tennessee, 2001.

133. Peng M, Jia H, Jiang L, et al. Study on structure and property of PP/TPU melt-blown nonwovens. *The Journal of The Textile Institute* 2018; 110: 468-475. DOI: 10.1080/00405000.2018.1485461.

134. Lee YE and Wadsworth LC. Fiber and web formation of melt-blown thermoplastic polyurethane polymers. *Journal of Applied Polymer Science* 2007; 105: 3724-3727. DOI: 10.1002/app.26432.

135. Molnar K and Meszaros L. The role of electrospun nanofibers in the fight against the COVID-19. *Express Polymer Letters* 2020; 14: 605-605. DOI: 10.3144/expresspolymlett.2020.49.

136. Czigany T and Ronkay F. The coronavirus and plastics. *Express Polymer Letters* 2020; 14: 510-511. DOI: 10.3144/expresspolymlett.2020.41.

137. Willeke K and Macher J. Bioaerosols: assessment and control. In: *Cincinnati, OH: American Conference of Governmental Industrial Hygienists* 1999.

138. Lee S-A, Adhikari A, Grinshpun SA, et al. Respiratory protection provided by N95 filtering facepiece respirators against airborne dust and microorganisms in agricultural farms. *Journal of Occupational and Environmental Hygiene* 2005; 2: 577-585.

139. Jafari M, Shim E and Joijode A. Fabrication of Poly (lactic acid) filter media via the meltblowing process and their filtration performances: A comparative study with polypropylene meltblown. *Separation and Purification Technology* 2021; 260: 118185.

140. Zhang H, Liu J, Zhang X, et al. Design of three-dimensional gradient nonwoven composites with robust dust holding capacity for air filtration. *Journal of Applied Polymer Science* 2019; 136: 47827.

141. Jackiewicz A and Werner L. Separation of nanoparticles from air using melt-blown filtering media. *Aerosol and Air Quality Research* 2015; 15: 2422-2435.

142. Zhang X, Liu J, Zhang H, et al. Multi-Layered, Corona Charged Melt Blown Nonwovens as High Performance PM0. 3 Air Filters. *Polymers* 2021; 13: 485.

143. Zhang H, Liu J, Zhang X, et al. Design of electret polypropylene melt blown air filtration material containing nucleating agent for effective PM2.5 capture. *RSC Advances* 2018; 8: 7932-7941. 10.1039/C7RA10916D. DOI: 10.1039/C7RA10916D.

144. Li T-T, Fan Y, Cen X, et al. Polypropylene/Polyvinyl Alcohol/Metal-Organic Framework-Based Melt-Blown Electrospun Composite Membranes for Highly Efficient Filtration of PM2. 5. *Nanomaterials* 2020; 10: 2025.

145. Liu C, Dai Z, He B, et al. The Effect of Temperature and Humidity on the Filtration Performance of Electret Melt-Blown Nonwovens. *Materials* 2020; 13: 4774.

146. Zhang H, Liu N, Zeng Q, et al. Design of Polypropylene Electret Melt Blown Nonwovens with Superior Filtration Efficiency Stability through Thermally Stimulated Charging. *Polymers* 2020; 12: 2341.

147. Zhang H, Zhen Q, Liu Y, et al. One-step melt blowing process for PP/PEG micro-nanofiber filters with branch networks. *Results in Physics* 2019; 12: 1421-1428. DOI: 10.1016/j.rinp.2019.01.012.

148. Kilic A, Shim E and Pourdeyhimi B. Electrostatic capture efficiency enhancement of polypropylene electret filters with barium titanate. *Aerosol Science and Technology* 2015; 49: 666-673.

149. Lou C-W, Shih Y-H, Huang C-H, et al. Filtration Efficiency of Electret Air Filters Reinforced by Titanium Dioxide. *Applied Sciences* 2020; 10: 2686.

150. Li T-T, Cen X, Ren H-T, et al. One-Step Bark-Like Imitated Polypropylene (PP)/Polycarbonate (PC) Nanofibrous Meltblown Membrane for Efficient Particulate Matter Removal. *Polymers* 2019; 11: 1307.

151. Zhang J, Chen G, Bhat GS, et al. Electret characteristics of melt-blown polylactic acid fabrics for air filtration application. *Journal of Applied Polymer Science* 2020; 137: 48309.

152. Yu B, Sun H, Cao Y, et al. Effects of Poly (ϵ-caprolactone) on Structure and Properties of Poly (lactic acid)/Poly (ϵ-caprolactone) Meltblown Nonwoven. *Polymer-Plastics Technology and Engineering* 2014; 53: 1788-1793.

153. Sellars WR. *Laminate non-woven sheet with high-strength, melt-blown fiber exterior layers*. USA, 2011.

154. Lim HS and Shin H. *Controlled-porosity, calendered spunbonded/melt blown laminates*. USA, 1994.

155. Gosavi N, Wadsworth LC and Duckett KE. Nonwoven Laminates Containing Cotton for Medical Applications. *Journal of Coated Fabrics* 1994; 24: 60-76.

156. Roh S, Park K and Kim J. Design of Web-to-Web Spacing for the Reduced Pressure Drop and Effective Depth Filtration. . *Polymers* 2020; 11: 1882.

157. Xiao H, Gui J, Chen G, et al. Study on correlation of filtration performance and charge behavior and crystalline structure for melt-blown polypropylene electret fabrics. *Journal of Applied Polymer Science* 2015; 132.

158. Myers DL and Arnold BD. Electret media for HVAC filtration applications. *International Nonwovens Journal* 2003: 1558925003os-1551200412.

159. Kowalski W, Bahnfleth WP and Whittam T. Filtration of airborne microorganisms: modeling and prediction. *ASHRAE TRANS* 1999; 105: 4-17.

160. EMI H, KANAOKA C, OTANI Y, et al. Collection mechanisms of electret filter. *Particulate science and technology* 1987; 5: 161-171.

161. Kilic A, Russell S, Shim E, et al. The charging and stability of electret filters. In: Brown PJ and Cox CL (eds) *Fibrous Filter Media*. United Kingdom: Woodhead Publishing, 2017, pp.95-121.

162. Yang Z, Lin J, Tsai I, et al. Particle filtration with an electret of nonwoven polypropylene fabric. *Textile research journal* 2002; 72: 1099-1104.

163. Brochocka A. Filtration Properties of Nonwoven Structures with Superabsorbents for Respiratory Protective Devices. *Fibres & Textiles in Eastern Europe* 2017.

164. Hossain E, Bhadra S, Jain H, et al. Recharging improves efficiency of decontaminated N95 masks. *arXiv preprint arXiv:200413641* 2020.

165. Majchrzycka K. Evaluation of a new bioactive nonwoven fabric for respiratory protection. *Fibres & Textiles in Eastern Europe* 2014.